# Spatial transcriptomics reveals injured cells, signature genes, and communication patterns in the cyst microenvironment of polycystic kidney disease

Yasinoglu, S.A.; Novella Rausell, C.; Wisse, L.E.; Dijkstra, K.L.; Mahfouz, A.; Baelde, H.J.; Peters, D.J.M.

OPEN

# Spatial Transcriptomics Reveals Injured Cells, Signature Genes, and Communication Patterns in the Cyst Microenvironment of Polycystic Kidney Disease

*Sevtap A. Yasinoglu*[1], *Claudio Novella-Rausell*[1], *Lisanne E. Wisse*[1], *Kyra L. Dijkstra*[2], *Ahmed Mahfouz*[1,3], *Hans J. Baelde*[2], *and Dorien J.M. Peters*[1]

## Key Points

- Myofibroblasts and injury repair–related cell types were exclusively observed in polycystic kidney disease and enriched within the cyst microenvironment.
- Cyst-associated gene signature of 45 genes with decreased expression further away from the cysts was largely related to inflammation.
- Communication in low-inflamed cystic microdomains related to cellular signaling, morphogenesis, and inflammation in polycystic kidney disease.

## Abstract

**Background** Changes in the cyst microenvironment in polycystic kidney disease (PKD) may drive progressive cyst formation. Bulk-cell and single-cell RNA sequencing have advanced our understanding of altered signaling; however, the lack of spatial information has limited our insights into local gene expression and cellular communication near cysts.

**Methods** We used wild-type and *Pkd1*-deficient mouse kidneys to generate 10× Genomics Visium Spatial Gene Expression datasets. Using our single-cell mouse kidney atlas and single-cell sequencing data for spot deconvolution, we enhanced resolution and estimated enriched cell types. We analyzed spatial gene expression patterns and used a cyst-centered analysis to identify cyst-associated gene signature. Cell communication near cysts was investigated, identifying key ligand-receptors. Prioritized key factors were validated in tissues.

**Results** We observed enrichment of fibroblasts, injury repair–related cell types, and diverse immune populations in PKD. Injury repair–related cells were exclusively observed in PKD, predominantly localized within immune cell–dense regions near cysts. These cells collectively contributed to the altered gene expression profile in PKD, including cyst-associated signature genes related to inflammatory processes. Analysis of cellular communication in less-inflamed regions around cysts revealed the involvement of multiple cell types. Key ligand-receptor interactions were associated with cytokine signaling, fibrosis, cellular development, and repair. These included *Angpt2*, *C3*, *Csf1*, *Cxcl12*, *Il34*, *Gas6*, *Il16*, *Mdk*, *Mif*, *Ptn*, *Sfrp2*, *Spp1*, *Sdc1*, *Tnc*, *Tnfsf12*, and *Wnt5a*. In addition, extracellular matrix (ECM) proteins implicated in immune response, ECM remodeling, cell adhesion, and cell signaling were identified, such as *Adam9*, *Adam10*, *Col1a1*, *Col3a1*, *Col4a2*, *Lamb2*, *Lamc1*, *Efnb1*, *Efnb2*, *Thbs1*, *Thbs2*, and *Vcam1*. Immunohistochemistry confirmed expression of Syndecan-1-Collagen IV, Midkine-Integrin $\beta$1, CSF-1, Pleiotrophin, and Tenascin-C in cystic kidneys.

**Conclusions** Spatial transcriptomics in PKD revealed enrichment of (myo)fibroblasts, immune, and injury repair–related cells near cysts, creating a (pro)inflammatory and (pro)fibrotic niche. Key ligand-receptor and ECM interactions were identified and validated.

*JASN* 00: 1–18, 2025. doi: https://doi.org/10.1681/ASN.0000000894



Due to the number of contributing authors, the affiliations are listed at the end of this article.

**Correspondence:** Prof. Dorien J.M. Peters, email: d.j.m.peters@lumc.nl

**Received:** October 24, 2024 **Accepted:** September 30, 2025
**Published Online Ahead of Print:** October 10, 2025

S.A.Y. and C.N.-R. contributed equally to this work.

  

## Introduction

Autosomal dominant polycystic kidney disease (ADPKD) is a genetic disorder with a prevalence of one in 2500 individuals.[1,2] Most patients carry a germ-line mutation in the *PKD1* (±78%) or *PKD2* (±15%) gene, encoding polycystin-1 or polycystin-2, respectively.[3–6] These mutations lead to progressive cyst formation and destruction of kidney parenchyma, resulting in a gradual decline in kidney function, and finally kidney failure.[7] Tolvaptan, a vasopressin V2 receptor antagonist, is the only US Food and Drug Administration–approved drug that slows the decline in kidney function.[8] To develop new therapies that preserve kidney parenchyma, a deeper understanding is needed of the molecular abnormalities in the cyst (micro) environment that contribute to progressive cyst formation.

In a slow-progressing mouse model of ADPKD, we previously showed that cyst formation was accelerated after the formation of initial cysts. These cysts were often surrounded by smaller cysts and exhibited altered PKD-related signaling in adjacent tissues.[9] RNA sequencing of microdissected tissues confirmed dysregulated signaling pathways in the cyst microenvironment, even before the accumulation of immune cells near cysts. Dysregulated pathways were related to injury repair processes, cell growth, tissue remodeling, and metabolism.[10] These data suggest that increased activity of paracrine factors in the cyst microenvironment may drive progressive cyst formation.[9,10] Accordingly, single-cell RNA sequencing of *Pkd1*-mutant kidneys revealed elevated expression of cytokines and their receptors in *Pkd1*-mutant cells, immune cells, and fibroblasts, indicating a positive feedback loop between *Pkd1*-mutant cells and surrounding cells that promote disease progression.[11] However, this study, as well as bulk-RNA sequencing studies, lack spatial information.[10–16] Thus, it remains unclear which cell types contribute to altered signaling near cysts and how cyst-lining cells communicate with neighboring cells to drive disease progression.

Here, we performed spatial transcriptome analysis in wild-type (WT) and PKD kidneys. This enabled us to map cell types and spatial gene expression patterns in both healthy and PKD kidneys. Through spot deconvolution, we refined the kidney cell-type composition and identified a robust gene expression signature for the cyst microenvironment. Furthermore, we investigated cell–cell communication near cyst-lining cells and uncovered key ligand-receptor pairs that may contribute to disease progression.

## Methods

### Animals

Animal experiment was approved by the Ethics Committee of Leiden University Medical Center and the Dutch Ministry of Agriculture (AVD1160020197684), following Directive 2010/63/EU. Tamoxifen-inducible kidney-specific *Pkd1*-deletion mice (iKsp*Pkd1*$^{del}$) were described before.[17] Scattered *Pkd1*-deletion was induced in male mice using 12.5 mg/kg oral tamoxifen administration on PN18-19.[10] PKD mice were sacrificed between PN264-297 and the WT mouse at PN284. Kidneys were collected, weighed, and either snap-frozen or fixed in formaldehyde.

### 10× Genomics Visium Spatial Gene Expression Experiment

Cryo sections of 10-$\mu$m thickness were placed on a precooled Visium Spatial Gene Expression slide (PN:2000233; SN:V10T17-045). Tissue fixation, hematoxylin & eosin (H&E) staining, and imaging were performed according to manufacturer's instructions. Imaging was conducted using ZEISS Axio Scan Z1. H&E stained sections were permeabilized for 12 minutes. Reverse transcription, cDNA synthesis, amplification (16–17 cycles), clean-up, quantification, and library construction were conducted according to manufacturer's instructions. Libraries were PCR amplified for 12 cycles and sequenced with 500 million 150 bp paired-end reads using NovaSeq 6000 v1.5.

### 10× Genomics Visium Spatial Gene Expression Raw Data Processing

Sequencing reads were mapped to the mm10 mouse genome (GRCm38) using Space Ranger v1.3.0 with manual fiducial alignment files. Count matrices were preprocessed with Scanpy[18] v1.8.1, merging samples and removing spots with >30% mitochondrial reads or <5000 counts, and genes expressed in <10 spots. A total of 8171 spots from capture areas were used for downstream analysis. Counts were normalized per spot at a target depth of 10,000 reads and log-transformed. The top 2000 highly variable genes were computed using seurat_v3 flavor and the batch key set to the different samples. Normalized counts were scaled before Principal Component Analysis. The top 50 principal components were used to create the neighborhood graph with Euclidean distance. For visualization, a two-dimensional uniform manifold approximation was computed using default parameters. Unsupervised clusters were identified using the Leiden algorithm[19] with a resolution of 0.7. Differential gene expression between clusters was analyzed using the Wilcoxon rank-sum test on the normalized counts.

### Gene Set Enrichment Analysis

Differential expression results were used for gene set enrichment analysis using fgsea v1.28.0[20] and gene sets from MSigDB v2023.2.Mm.[21] Ranked list of genes or ligand-receptor pairs identified overrepresented and underrepresented gene sets. Normalized enrichment scores allowed comparisons across gene sets. To reduce redundancy, rrvgo v1.2.0[22] was used with a semantic similarity threshold of 0.25. An adjusted $P$ value $< 0.05$ was considered significant.

### Spatial Pattern Analysis

Log-normalized counts were used as input for Mefisto (mofapy2 v0.7.0),[23,24] and 15 spatial patterns (*i.e.*, factors) per kidney were obtained using the highly variable genes identified previously. We computed spatial covariance using 1000 inducing points.

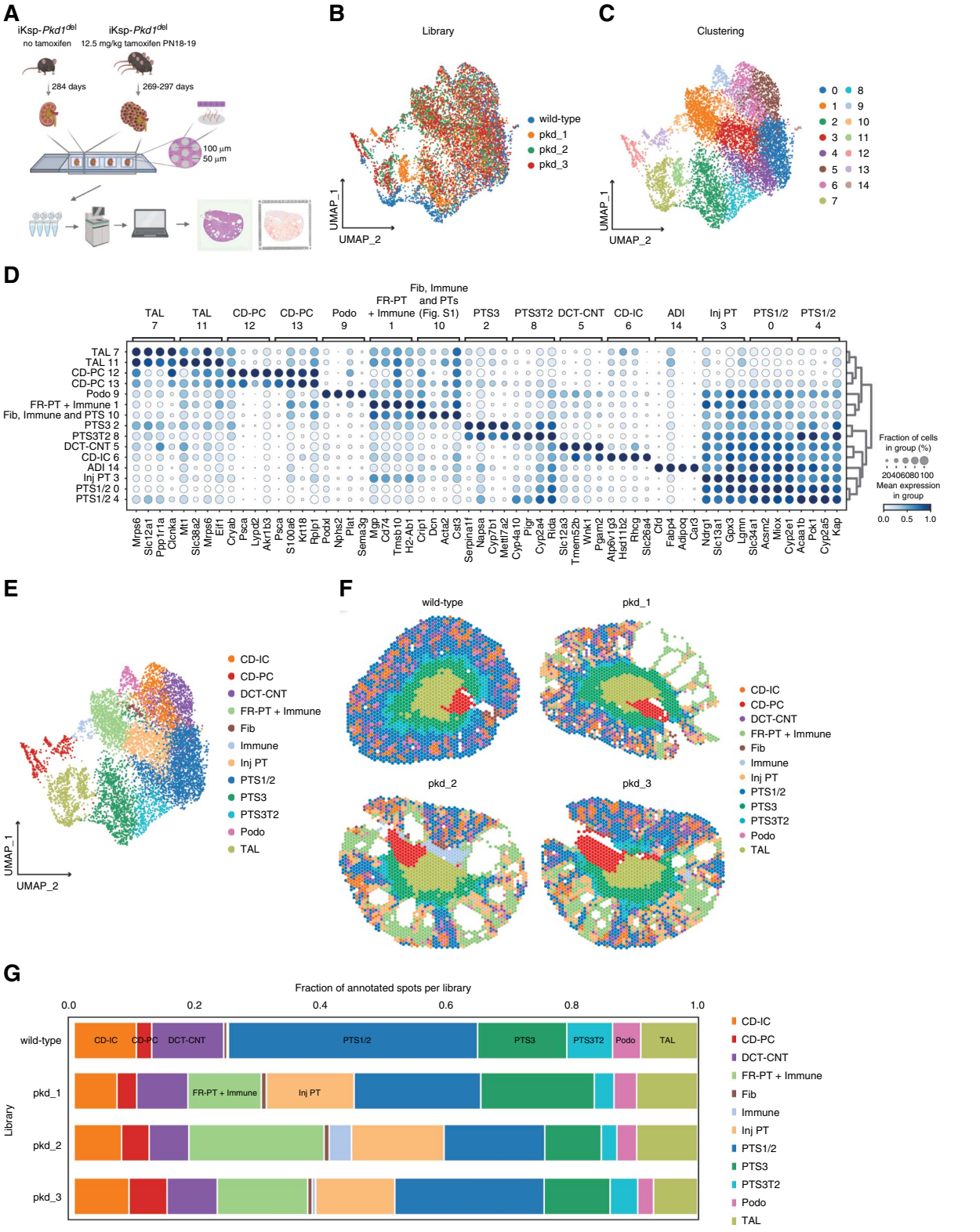


**Figure 1. Spatial gene expression analysis and identification of major cell-type clusters in wild-type and PKD kidneys and their spatial localization.** (A) Schematic overview of the experimental design, 10× Visium library construction, and data acquisition. In brief, fresh frozen kidney sections from male C57BL/6 mice were used with scattered *Pkd1* deletion (iKsp*Pkd1*$^{del}$, 12.5 mg/kg tamoxifen PN18-19, $n$=3) and age-matched wild-type mouse (iKsp*Pkd1*$^{del}$, no tamoxifen, $n$=1). Frozen kidney sections were placed onto spatially barcoded slides, fixated, stained with H&E, and imaged. Upon permeabilization, the polyadenylated mRNA was released from the overlying cells and captured by the primers on the spots (typically from 1 to 20 cells). After second-strand synthesis and cDNA amplification, cDNA libraries were generated and sequenced. Raw sequencing data were transformed into gene expression data and aligned with the H&E

**Figure 1.** *Continued.* images of the kidney sections. (B) UMAP visualization colored by kidney-library (wild-type, pkd_1, pkd_2, pkd_3). (C) UMAP visualization colored by unsupervised clusters (0–14). Each dot represents a sequenced Visium spot. (D) Dotplot visualization of the top four DEGs per cluster. See Supplemental Table 1 for a complete DEGs list. (E) UMAP visualization colored by cell-type annotation. Based on similar gene expression profiles, Clusters 7 and 11 and 12 and 13 from panel C were grouped into one cell type each. Cluster 14 was annotated as adipocytes, derived from some fat tissue outside the medulla, and excluded from downstream analysis. Cluster 10 was subclustered, improving separation of Fib cluster from proximal tubule and immune (Supplemental Figure 1 and Supplemental Table 1). (F) Visium spots colored by annotation. (G) Stacked bar plot displaying the fraction of annotated spots per kidney. Exact proportions are presented in Supplemental Table 2. ADI, adipocytes; CD-IC, collecting duct intercalated cells; CD-PC, collecting duct principal cells; CNT, connecting tubule; DCT, distal convoluted tubule; DEG, differentially expressed genes; Fib, fibroblast; FR-PT, failed repair PT; H&E, hematoxylin & eosin; immune, immune cells; Inj PT, injured PT; PKD, polycystic kidney disease; Podo, podocyte; PT, proximal tubule; PTS1, PT segment 1; PTS2, PT segment 2; PTS3, PT segment 3; PTS3T2, PT segment 3 type 2; TAL, thick ascending limb of the loop of Henle (LOH); UMAP, uniform manifold approximation.

### Visium Spot Deconvolution

Spot deconvolution was performed using Tangram v1.0.2[25] with modified mouse kidney atlas (MKA) as a reference. The original MKA atlas (github.com/nrclaudio/MKA)[26] was enriched with immune,[27] injury-induced populations,[28] as well as PKD[16] transcriptomic profiles from additional datasets (GSE190887, GSE193528, and GSE268494). Batch correction between the original MKA data and the three additional datasets was done using scVI (scvi-tools v0.14.3[29]), followed by scANVI.[30] In each deconvolution task, we accounted for differences in cell-type proportions between our reference and the target slide using Seurat v3.[31] Details are presented in Supplemental Material.

### Cyst Border Identification and Gene Expression Models

Cysts in each PKD kidney were manually segmented. Cyst borders were identified using scikit-image v0.22.0, and distances from segmented nuclei to nearest cyst were computed using scipy.spatial.cKDTree. Generalized Additive Models were fit for each gene using PyGAM v0.9.0. A cyst-associated gene signature was derived by identifying genes with rapid expression decline near cysts and low expression far from cysts, intersected across PKD kidneys. A cyst-associated gene score was calculated using Overrepresentation Analysis with the Fisher exact test, based on the overlap between highly expressed genes in each spot and the cyst-associated gene signature. Details are presented in Supplemental Material.

### Cell Communication

LIANA+ (lianapy v0.1.8)[32] was used to compute cell–cell communication scores between cell types in immune-low contexts around cysts. Three layers around cysts were manually defined to study communication events by distance. An expression threshold was applied, requiring at least 85% of spots in a specific cell type to express the ligand and receptor, with gene expression levels at least twice as high as in noncystic areas. Details are presented in Supplemental Material.

### Immunohistochemistry

Sections of 4-$\mu$m thickness underwent antigen retrieval and blocking of endogenous peroxidases with 0.1% $H_2O_2$ and then incubated with primary and secondary antibodies. Immune reactions were revealed using Fast Red substrate kit (ab64254), 3,3′-diaminobenzidine (ab64238) or 3,3′-diaminobenzidine+ (K3468), and counterstained with Mayer hematoxylin. Details are presented in Supplemental Material.

## Results

### Spatial Transcriptomics of WT and PKD Kidneys and the Identification of Unsupervised Major Cell-Type Clusters

To explore distinct cell types in the cyst microenvironment in PKD, sections from one WT and three PKD kidneys with scattered *Pkd1*-deletion[10] were analyzed using 10× Genomics Visium platform (Figure 1A). An overview of the analyzed number of spots, mean reads per spot, median genes per spot, the number of reads, and genes per kidney is presented in Supplemental Methods. No batch effects were observed between the libraries (Figure 1B). Unsupervised clustering was performed at the spot level, with clusters annotated using top differential genes and cell-type markers from previous studies (Figure 1, C and D, and Supplemental Table 1).[26,28,33] This resulted in 12 major cell types, with some clusters merged based on shared gene expression profiles (clusters 7 and 11; 12 and 13) and removal of cluster 14 (adipocytes) (Figure 1E and Supplemental Figure 1A). In addition, subclustering of cluster 10 refined the separation of Fib, immune, and proximal tubule (PT) clusters (Figure 1, D and E, and Supplemental Figure 1B). These were projected onto the tissue sections to visualize distribution in different kidney segments (Figure 1F). Interestingly, PT-FR+Immune and PT-Inj clusters were exclusively located near cysts in PKD kidneys, while absent in the WT kidney (Figure 1, F and G). Moreover, the fraction of proximal tubule clusters was reduced in PKD kidneys (Figure 1G and Supplemental Table 2). Previously, failed repair proximal tubule (PT-FR) cells were identified as a cell state that failed to repair after acute injury, exhibiting proinflammatory and profibrotic features.[34] Enrichment of PT-Inj and PT-FR+Immune clusters, primarily within the cyst microenvironment, suggests the presence of proinflammatory and profibrotic niches in PKD kidneys, while noncystic regions resemble the WT kidney.

### Deconvolution Defined Cell-Type Composition of the Spots in WT and PKD Kidneys

To enhance cellular resolution, we performed cell-type deconvolution and nuclei segmentation. We enriched our single-cell MKA[26] with immune,[35] injured,[28] and cystic[16] cells, creating a reference composed of 50% healthy cells and 50% injured, fibrotic, cystic, and immune cells. A list of meta-markers used

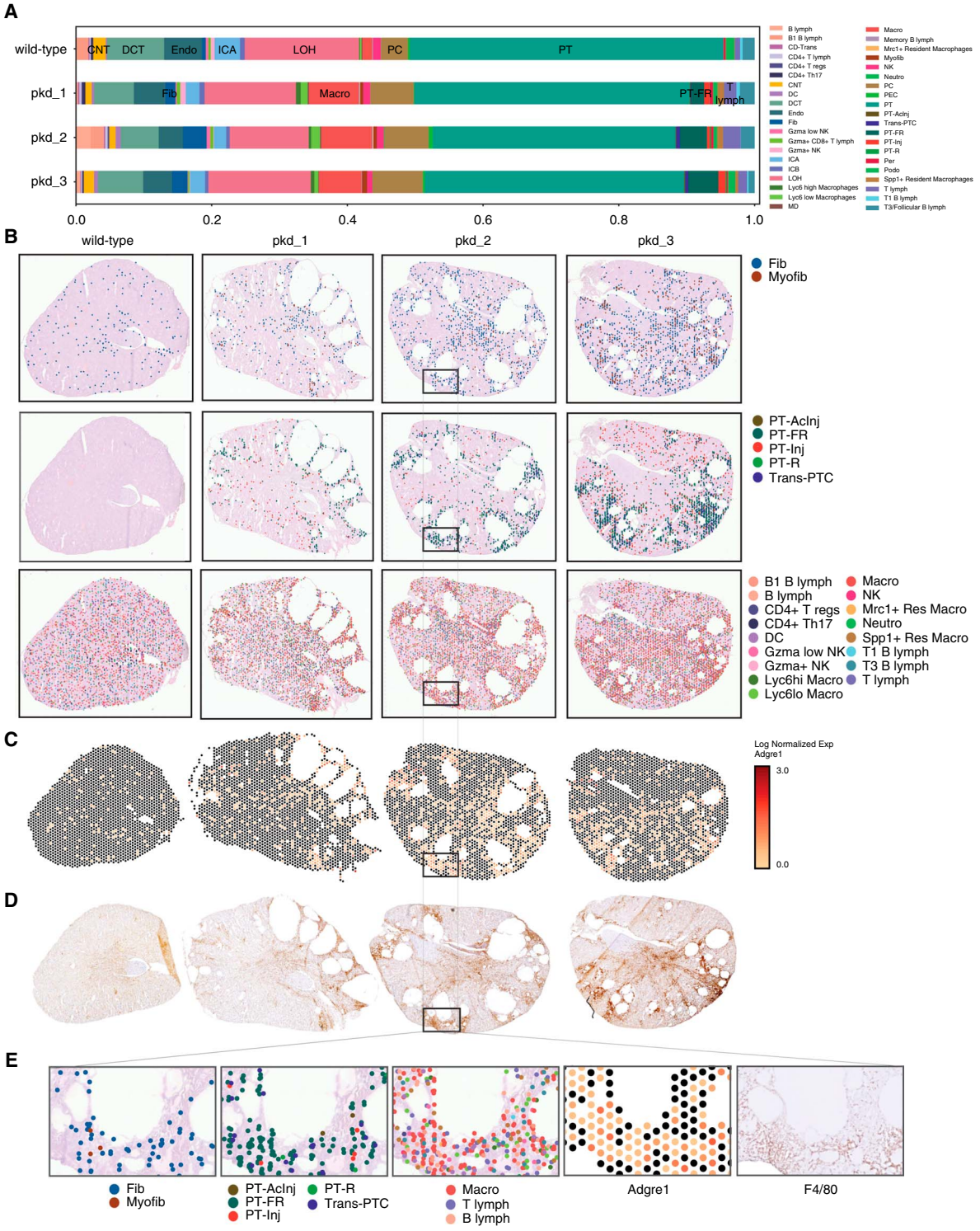


**Figure 2. Cell-type deconvolution reliably defines cell-type composition of the spots identifying less abundant cell types.** (A) Stacked bar plot displaying the fraction of annotated nuclei after deconvolution. Major cell types are indicated in the bars. Exact proportions are presented in Supplemental Table 2. (B) Segmented nuclei colored by their deconvoluted cell types: Fib/Myofib, PT injured cell states, or immune cell populations in wild-type and PKD kidneys. Every dot is a single cell type (annotated segmented nucleus), identified in barcoded spots. (C) Spatial expression pattern for murine macrophage/monocyte marker *Adgre1*. We only plot spots in which *Adgre1* expression is detected (>0), in orange-red color scale. (D) IHC staining of F4/80 murine monocyte/macrophage marker in kidney sections adjacent to the Visium dataset. (E) Magnification of a region near cyst with different cell populations, as well as expression of the *Adreg1* gene and F4/80 IHC in a section adjacent to the Visium dataset. B Lymph, B lymphocyte; B1 B lymph, B1 B lymphocyte; CD-Trans, collecting duct transitional population; $CD4^+$ Th17, $CD4^+$ T helper 17; $CD4^+$ T regs, $CD4^+$ regulatory T; DC, dendritic cells; Endo, endothelial; Gzma low NK, Gzma low natural killer; Gzma+NK, Gzma+natural killer; ICA, intercalated cell type A;

**Figure 2.** *Continued.* ICB, intercalated cell type B; IHC, immunohistochemistry; Lyc6 high macro, Lyc6 high macrophage; Lyc6 low macro, Lyc6 low macrophage; macro, macrophage; MD, macula densa; Mrc1+ resident macro, Mrc1+ resident macrophage; Myofib, myofibroblast; Neutro, neutrophil; NK, natural killer; PC, principal cell; PEC, parietal epithelial cell; per, pericyte; PT-AcInj, acute injury PT; PT-FR, failed repair proximal tubule; PT-Inj, injured PT; PT-R, repairing PT; Spp1+ Resident Macro, Spp1+ resident macrophage; T lymph, T lymphocyte; T1 B Lymp, T1 B lymphocyte; T3/follicular B lymph, T3/follicular B lymphocyte.

to characterize the cell types in this reference is presented in Supplemental Table 2; however, these were not used for annotation or any downstream analysis. This enriched reference enabled estimation of cell-type composition in WT and PKD kidneys (Supplemental Figures 2–5). Compared with the WT, PKD kidneys showed increased proportions of myofibroblasts, immune populations, and injury repair–related cell states (Figure 2A and Supplemental Table 3). The increased proportion of injury repair–related cell types aligns with the previously reported proportions in PKD.[36] Nuclei annotated as Fib and immune cell types were sparse and randomly distributed throughout WT kidney, while increased and concentrated near cysts in PKD kidneys (Figure 2B, Supplemental Figures 6–9). Among the deconvoluted immune cell populations, macrophages constituted the majority (Figure 2), confirmed by *Adgre1* gene expression and F4/80 staining (Figure 2, B–E, and Supplemental Figure 10A). Myofibroblasts and B/T lymphocytes were also enriched near cysts, although less prevalent (Figure 2E). This was confirmed by αSMA (activated fibroblasts), CD3 (T lymph), and CD19 (B lymph) stainings in PKD kidneys (Supplemental Figure 10B). Transitional proximal tubule cells (Trans-PTC) were exclusive to PKD kidneys (Figure 2A and Supplemental Table 2). PT-AcInj, PT-Inj, and PT-R cells were previously characterized by downregulation of healthy proximal tubule markers and upregulation of heat-shock proteins, tubule injury, and cell proliferation markers, while Trans-PTCs only downregulated proximal tubule markers, suggesting a transitional phase.[16,28,34] These findings highlight cellular remodeling predominantly within the cyst microenvironment in PKD, including increased proportions of immune cells, myofibroblasts, injured, and transitioning cell types.

### Identification of Spatial Gene Expression Patterns in WT and PKD Kidneys

We applied MEFISTO[24] to investigate spatial gene expression patterns using unsupervised factor analysis, identifying up to 25 patterns (Supplemental Figures 11–14 and Supplemental Table 4). Using the top 2000 variable genes, we assessed factor correlation across kidneys (Figure 3A). Several factors correlated among the kidneys, revealing shared spatial expression profiles between the medullary regions and noncystic cortical regions in PKD and WT kidneys (Figure 3, A and B). Despite these similarities and overlapping marker genes, an additional enrichment pattern emerged around cysts, particularly in Factor 1 (Figure 3B).

We evaluated the top 50 variable genes for Factor 1 to assess the most pronounced differences between WT and PKD kidneys (Figure 3C and Supplemental Table 4). These genes showed markedly altered gene expression in the cyst microenvironment. Among the top 50 lower-expressed genes in PKD cyst microenvironment were *Acaa1b, Chpt1, Rida, Slc7a13, Acy3,* and *Cyp2a4*, which are involved in metabolism and transport (Figure 3C). By contrast, the top 50 higher-expressed genes were associated with PT-FR+Immune cell cluster (Figure 1D: *Mgp, Cd74,* and *Tmbs10*), proximal tubule injury, macrophage-related genes *Lcn2*,[37] *Apoe*,[27,38] and *Spp1*,[38,39] and inflammatory pathways (Figure 3C). Among PKD kidneys, Pkd_2 showed the strongest divergence from WT compared with Pkd_1 and Pkd_3 kidneys, likely due to a higher abundance of cystic clusters. Consistently, gene ontology (GO) term analysis of Factor 1 showed significant enrichment for immune response, response to wounding, cytoskeletal changes, cell migration, and reduced metabolism in PKD (Figure 3D). Together, major transcriptomic changes reflected by Factor 1 are primarily located near cyst clusters, although gene expression profiles are highly correlated across whole kidney sections in WT and PKD. This suggests that in noncystic regions, scattered *Pkd1* deletion and sparse immune/injured cells do not drive broad transcriptomic shifts.

### Characterization of Gene Expression and Cell-Type Distribution within Cyst Microenvironment

Given both segment-specific and cyst microenvironment-related changes in spatial gene expression (Figure 3), we used a cyst-centered approach for further investigation. We manually segmented the cysts and computed the distance of each segmented nucleus (randomly distributed within a spot) to its nearest cyst per kidney (Figure 4A). Using deconvolved cell types and segmented nuclei, we estimated cell populations closest to the cysts. Parietal epithelial cell, PT-FR, and Trans-PTC were closest to the cysts, followed by various immune cells, (myo)fib, and injury-related cells (Figure 4B). Among the cell types closest to the cysts, PT-FR and immune cells were relatively the most abundant (Supplemental Figure 15). We modeled gene expression per spot based on its distance to the nearest cyst, identifying 45 signature genes with high expression near cysts that decreased with distance (Figure 4C and Supplemental Figures 22–23). We will refer to these genes as cyst-associated signature genes. These include genes already discussed above (*e.g., Cd74, Mgp, Tmsb10, Lcn2, Apoe*), complement C1q regulation (*C1qa, C1qb, C1qc, Serping1*), antigen presentation (*H2-Aa, H2-Ab1, H2-Eb1, Ctss, B2m, Fcer1g*), or extracellular matrix (ECM) organization/degradation (*Col1a1, Col1a2, Col3a1, Fn1, Timp2, Bgn*). Furthermore, clusterin (*Clu*) has previously been identified in cyst-lining epithelial cells across various cystic kidney diseases, as well as in immature nephrons and injured tubules.[40] In addition, upregulation of Galectin-1 (*Lgals1*) and Vimentin (*Vim*) has been reported in renal

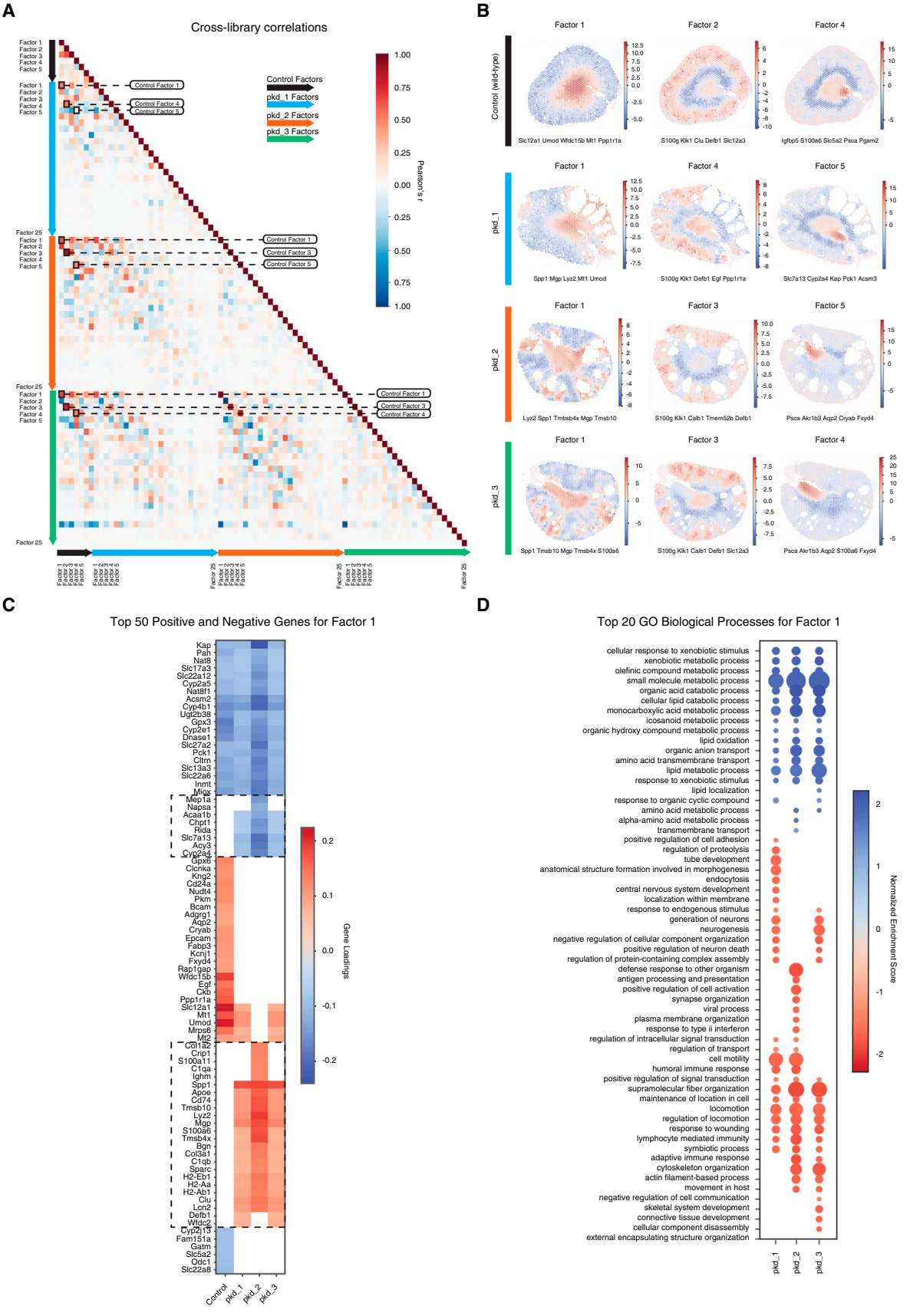
A
Cross-library correlations
Control Factors
pkd_1 Factors
pkd_2 Factors
pkd_3 Factors
Pearson's r
B
Control (wild-type)
pkd_1
pkd_2
pkd_3
C
Top 50 Positive and Negative Genes for Factor 1
Gene Loadings
Control
pkd_1
pkd_2
pkd_3
D
Top 20 GO Biological Processes for Factor 1
Normalized Enrichment Score

**Figure 3. Spatial gene expression pattern analysis reveals a distinct gene expression profile in the cyst microenvironment.** (A) The top 2000 genes per factor per kidney were ranked based on gene loadings, and Pearson correlation was calculated between factors identified per kidney. (B) Visium spots from the wild-type, pkd_1, pkd_2, and pkd_3 kidneys colored by highly correlating factors across kidneys as highlighted in (A). Of note: factors have been created per individual kidney and are not identical across different kidneys. The top five genes with the highest factor weight are shown per factor per kidney. See Supplemental Table 4 for a complete list of the genes per factor per kidney. (C) Heatmap displaying the genes with the highest and lowest (top 50) weights for Factor 1 per kidney. Blanks represent genes that were not among the top 50 (highest or lowest) in the given kidney. Dashed boxes indicate genes that are consistently in the top 50 in PKD kidneys and not in wild-type. Genes are clustered by their gene weights. (D) Dot plot of the significant (adjusted $P$ value $<0.05$) gene set enrichment results for Factor 1 gene weights in PKD kidneys. The top redundancy-reduced GOBP terms by both positive (top 20) and negative (top 20) with NES are visualized per kidney. Rows are clustered by NES. GOBP, gene ontology biologic processes; NES, normalized enrichment score; SPARC, secreted protein acidic and rich in cysteine.

epithelial cells in autosomal recessive polycystic kidney disease.[41] In ADPKD, Clusterin, complement factor H (*Cfh*), prostaglandin D2 synthase (*Ptgds*), and *Serping1* have been detected in cyst fluid.[42] Elevated levels of secreted protein acidic and rich in cysteine have been found in both the cyst fluid and urine of ADPKD patients, with localization primarily in cyst-lining epithelial cells and dilated tubules.[43] Several additional factors identified in our dataset, such as *Anxa2*,[44] *Cxcl16*,[45] and *Timp2*,[46] have previously been linked to CKD.

Notably, some genes also show elevated expression at intermediate distances from cysts. These genes are also expressed in the outer medulla and reflect spots that are at a longer distance from the cysts. We correlated the cell-type abundance with the cyst-associated gene signature score per spot and found associations with Macro, Fib, T lymph, and PT-FR cells (Figure 4D). These findings confirm the (pro)inflammatory and (pro)fibrotic milieu within the cyst microenvironment, highlighting a set of robustly enriched genes and closely associated cell types adjacent to the cysts.

### Unraveling Cell–Cell Communication Events in the Cyst Microenvironment

To investigate cell–cell communication in the PKD cyst microenvironment, we annotated spots around cysts into three layers. The first layer consists of spots directly lining the cysts, the second layer surrounds the first, and the third layer surrounds the second (Figure 5A). We prioritized ligand-receptor pairs with at least twice the expression in these layers compared with spots in noncystic regions. Using deconvolved immune cell composition and *Adgre1* (F4/80) expression, we distinguished immune cell low and high spots around cysts in every layer (Figure 5A, bottom panel). We primarily focused on interactions within immune-low spots, based on unsupervised cell-type annotations (as shown in Figure 1F). Each predominant cell type could act as both a sender and receiver, based on ligand and receptor expression. Immune-low spots, while capturing gene expression profiles from multiple cells, including immune, injured, and failed repair proximal tubule cells, contain a higher proportion of epithelial cells, as determined by segmented nuclei counts and deconvolution analysis (Figure 5B). These epithelial cells have presumably not (yet) adopted a cystic or failed repair phenotype and may represent an earlier or pretransitional state. Therefore, analyzing these spots may reveal signals more likely to be perceived by epithelial cells in a putative precystic state, potentially contributing to cyst initiation under prolonged stimulation.

This analysis identified 11 factors capturing cell–cell communication and ligand-receptor interactions across three layers surrounding cysts in PKD kidneys (Supplemental Figure 16 and Supplemental Table 5). We evaluated Factors 2 and 6, showing opposing enrichment patterns in the analyzed layers: Factor 2 was enriched in the third layer in all three kidneys, while Factor 6 was primarily enriched in layers 1 and 2 (Figure 5, C and D). One PKD kidney (Pkd_3) differed in layer 2 for both factors, likely due to the smaller cysts. Figure 5, C–F, shows the contribution of major cell types to cell–cell communication. Near cysts (Factor 6), Fib and PT-FR+Immune cells predominantly received signals, and to a lower extent Inj PT, PTS3T2, CD-IC, and DCT-CNT. In the surrounding tissue (Factor 2), a wider variety of cell types were stimulated at equal levels.

To evaluate the biologic processes associated with the identified cell–cell communication factors, we analyzed whether ligand-receptor pairs were enriched in specific GO terms. Owing to the limited number of enriched ligand-receptor pairs surrounding cysts (excluding genes that were neither ligands nor receptors), the normalized $P$ values for the enriched GO terms were significant, but the false discovery rate–adjusted q-values were $>0.05$. Nevertheless, our enrichment data provide insights into the linked biologic processes (Supplemental Table 6). Near cysts (Factor 6), enriched processes were associated with immune system development, regulation, and immune cell migration, highlighting roles in immune responses, and also involve cell activation and cellular signaling (Figure 5G). More distant from cysts (Factor 2), enriched processes involve cell morphogenesis, differentiation, immune system regulation, and vesicle-mediated transport, emphasizing roles in development, immune response, and cellular transport (Figure 5G). These findings indicate active immune-related processes within the cyst microenvironment, even in immune-low regions, and underscore enhanced cellular signaling, differentiation, and morphogenetic activity.

### Identification and Validation of Key Ligand-Receptor Pairs

We evaluated the top 20 ligand-receptor pairs contributing to cell communication in immune-low spots, as captured by Factors 2 and 6 (Supplemental Table 5). Identified ligands include secreted paracrine factors that, in relation to their receptors, are associated with cytokine signaling, fibrosis, cell development, and repair, including *Angpt2*,[47] *C3*,[48] *Csf1*,[49] *Cxcl12*,[50] *Il34*,[49] *Gas6*,[37] *Il16*,[51] *Mdk*,[52–55] *Mif*,[56] *Ptn*,[57,58] *Sfrp2*,[59] *Spp1*,[39] *Sdc1*[60], *Tnfsf12*,[61] and *Wnt5a*.[62,63] In addition, several proteins involved in ECM remodeling,

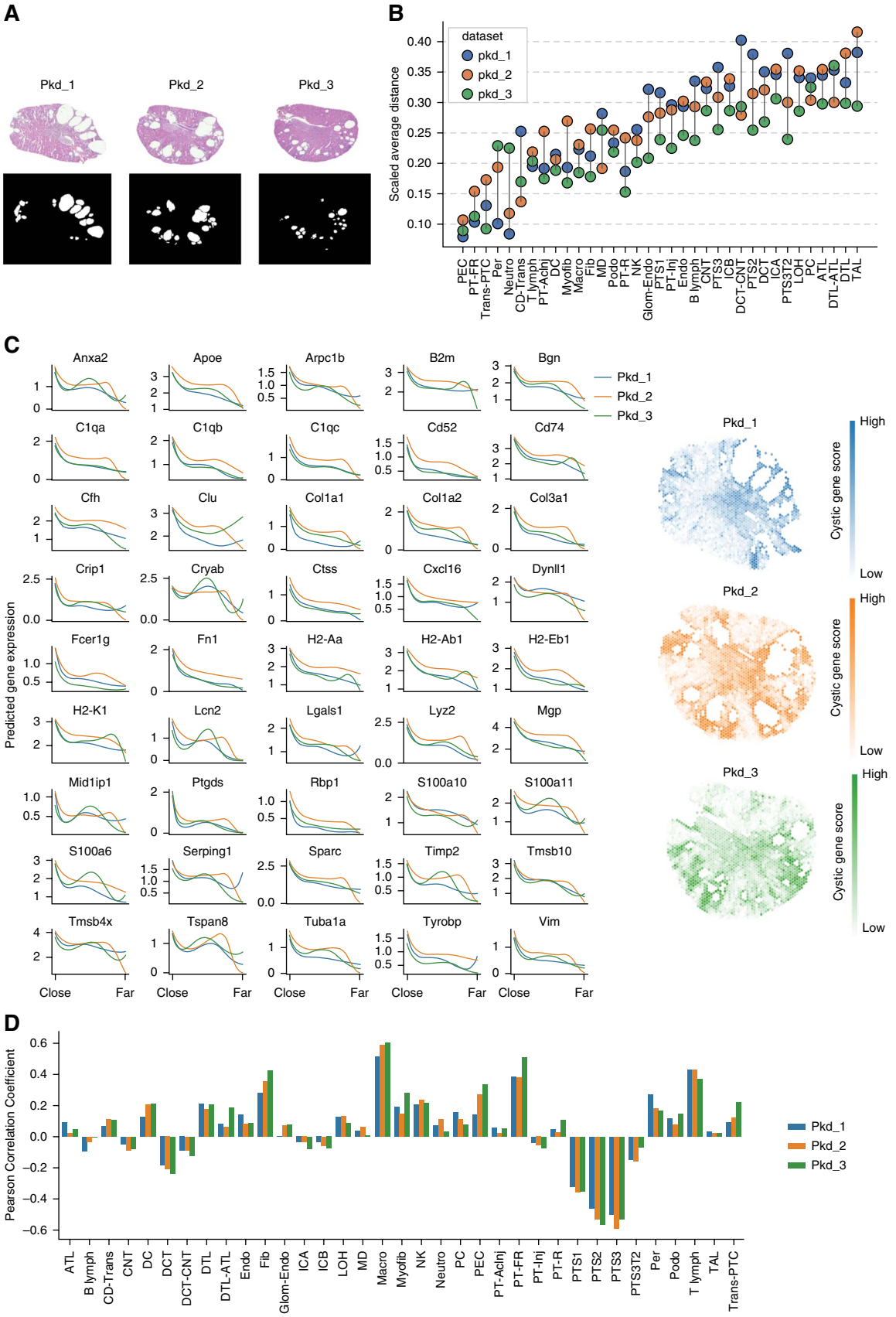
A
Pkd_1
Pkd_2
Pkd_3
B
dataset
pkd_1
pkd_2
pkd_3
Scaled average distance
PEC
PT-FR
Trans-PTC
Per
Neutro
CD-Trans
T lymph
PT-AcInj
DC
Myofib
Macro
Fib
MD
Podo
PT-R
NK
Glom-Endo
PTS1
PT-Inj
Endo
B lymph
CNT
PTS3
ICB
DCT-CNT
PTS2
DCT
ICA
PTS3T2
LOH
PC
ATL
DTL-ATL
DTL
TAL
C
Predicted gene expression
Anxa2
Apoe
Arpc1b
B2m
Bgn
C1qa
C1qb
C1qc
Cd52
Cd74
Cfh
Clu
Col1a1
Col1a2
Col3a1
Crip1
Cryab
Ctss
Cxcl16
Dynll1
Fcer1g
Fn1
H2-Aa
H2-Ab1
H2-Eb1
H2-K1
Lcn2
Lgals1
Lyz2
Mgp
Mid1ip1
Ptgds
Rbp1
S100a10
S100a11
S100a6
Serping1
Sparc
Timp2
Tmsb10
Tmsb4x
Tspan8
Tuba1a
Tyrobp
Vim
Close
Far
Pkd_1
Pkd_2
Pkd_3
Cystic gene score
High
Low
D
Pearson Correlation Coefficient
ATL
B lymph
CD-Trans
CNT
DC
DCT
DCT-CNT
DTL
DTL-ATL
Endo
Fib
Glom-Endo
ICA
ICB
LOH
MD
Macro
Myofib
NK
Neutro
PC
PEC
PT-AcInj
PT-FR
PT-Inj
PT-R
PTS1
PTS2
PTS3
PTS3T2
Per
Podo
T lymph
TAL
Trans-PTC
Pkd_1
Pkd_2
Pkd_3

**Figure 4. Characterization of gene expression and cell-type distribution near cysts identifies cystic microenvironment-specific gene signature.** (A) Manually segmented cysts in PKD kidneys used to calculate the distance of each segmented nuclei to its nearest cyst. (B) Scatterplot of the average distance of each cell type to its nearest cyst. (C) Line plots of the predicted gene expression trends (the pattern lines) over normalized distance to the cyst for the 45 common cyst-associated (signature) genes in each PKD kidney (left). Spatial plots of the computed cyst-associated signature score in each PKD kidney (right). (D) Bar plots displaying the Pearson correlation coefficients (r) between the abundance of each deconvolved cell type and the cyst-associated signature gene score for each of the PKD kidneys. ATL, ascending thin limb; DTL, descending thin limb; Glom-Endo, glomerular endothelial cell.

cell adhesion, and cell signaling were identified, including *Adam9*,[64] *Adam10*,[65] *Cola1a, Col3a1, Col4a2, Lamb2, Lamc1, Efnb1*,[66] *Efnb2*,[66] *Thbs1, Thbs2*, and *Vcam1*.[67] Increased expression of these ECM proteins and their interaction with receptors (mainly integrins) could also activate proproliferative and profibrotic pathways.[68]

Although not our primary focus, we additionally evaluated ligand-receptor pairs driving cell communication in immune-high and immune-low spots (Supplemental Figure 17 and Supplemental Table 7). Among the ten newly generated factors, Factor 2 exhibits high activity in immune-high spots and low activity in immune-low spots. The top contributors to cell communication in immune-high spots include ECM and cell adhesion molecules (*Col1a1, Col5a1, Col12a1, Col14a1, Col18a1, Fn1, Icam1*, and integrins), complement factors (*C3, Cfh*), and Semaphorin 3, mostly associated with a stromal microenvironment, aligning with the immune cell–high cyst microenvironment.[69]

In addition, we performed a differential gene expression analysis comparing ligand-receptor pairs in immune-high and immune-low spots, including ligand-receptor pairs for which both the ligand and receptor were differentially expressed, as well as those in which only the ligand or only the receptor showed differential expression. This yielded 317 ligand-receptor pairs with significantly higher expression in immune-high spots compared with immune-low spots, along with 793 ligand-only and 508 receptor-only pairs. Comparing immune-low to immune-high spots yielded only five ligand-receptor pairs (Supplemental Table 8).

Further focusing on the immune-low layers, we analyzed the overlap between our top ligand-receptor pairs (gene weight above 0.06, Supplemental Table 5) and differentially expressed protein-coding genes from the cilia-dependent cyst activation pattern identified in a recent study.[70] This pattern includes actively translated genes (440 differentially expressed genes [DEG] in male and 526 DEGs in female mice) in precystic kidneys, regulated by the polycystin complex in cilia that requires intact cilia for its full function.[70] We identified 14 overlapping genes, including paracrine factors (*Ccl5, Egf, Lgals1*, and *Tnfsf13*) and receptors (*Csf1r, Tnfrsf10b*; Supplemental Figure 18, A and B). Furthermore, Sdc1, Csf1r, and Hfe were also among the top 20 ligand-receptor pairs, suggesting a higher contribution to the communication pattern identified by Factors 2 and 6 (Supplemental Figure 18C).

Based on spatial gene expression, pathogenic relevance, and antibody availability, we validated SDC1-COL4A1, colony-stimulating factor 1 (CSF1), MDK-ITGB1, Pleiotrophin (PTN), and Tenascin-C (TNC) by immunohistochemistry in mouse and/or human tissues. Syndecan-1 (SDC1, CD138), a transmembrane heparan sulfate proteoglycan, is expressed on epithelial cells and can be shed, influencing kidney injury, repair, and inflammation.[60] In healthy human kidneys, it is localized to the cytoplasm and primary cilia of tubular epithelial cells, with the strongest expression in proximal tubules and variable expression in distal segments (Figure 6A and Supplemental Figure 19A). Syndecan-1 is known to interact with several ECM components and paracrine factors.[71] Our factor analysis highlights its association with Collagen IV (*Col4a2*, *Col4a4*). In ADPKD, Syndecan-1 expression is increased in dilated tubules near cysts, although ciliary localization was lost. Fibrotic regions adjacent to large cysts and atrophic tubules showed minimal Syndecan-1 expression, while collagen IV remained strongly expressed. This likely underlies the heterogeneous costaining pattern of Syndecan-1 and Collagen IV observed in dilated tubules (Figure 6A and Supplemental Figure 19A). Overall, Collagen IV staining was consistently high in both normal and dilated tubules of control and ADPKD kidneys.

CSF1 and IL 34 signal through the CSF1 receptor (CSFR) to regulate macrophage proliferation and differentiation.[49] Inhibition of CSF1-mediated resident macrophage proliferation was previously shown to reduce cyst formation in the kidneys.[72] In our analysis, CSF1 exhibited predominantly cytoplasmic staining in tubular epithelial cells. Its expression was broadly detectable throughout the kidney, particularly in healthy mouse tissue, and to a lesser extent in human controls (Figure 6B). However, both PKD and ADPKD samples showed markedly elevated CSF1 expression, including cyst-lining epithelia and surrounding tubules, suggesting disease-associated upregulation (Figure 6B).

Osteopontin (SPP1) is a highly expressed cytokine in tubular and cystic epithelial cells in PKD. Although its deletion suppresses cyst growth, it also promotes fibrosis.[73] Our data suggest SPP1 interacts with Integrins $\alpha5$ and $\beta1$. Another top-ranked protein, Midkine (MDK), a heparin-binding growth factor involved in cell survival, migration, epithelial–mesenchymal transition, and oncogenesis,[52,74] also associates with Integrin $\beta1$. Extracellular MDK can be internalized and translocated to the nucleus, where it exerts its prosurvival[75] or profibrotic[53] effects. In both normal and cystic kidneys (mouse and human), MDK showed strong nuclear and weaker cytoplasmic expression (Figure 6C and Supplemental Figure 19B). In cystic kidneys, its signal intensified in the cyst microenvironment, including infiltrating and interstitial cells, and colocalized with diffuse Integrin $\beta1$ expression (Figure 6B). While MDK expression was comparable between species, Integrin $\beta1$ expression was more prominently expressed in glomeruli and tubular basement membranes in ADPKD.

TNC (Factor 2, Top 33), a key mediator in fibrogenic niche formation and loss of tubular integrity in CKD

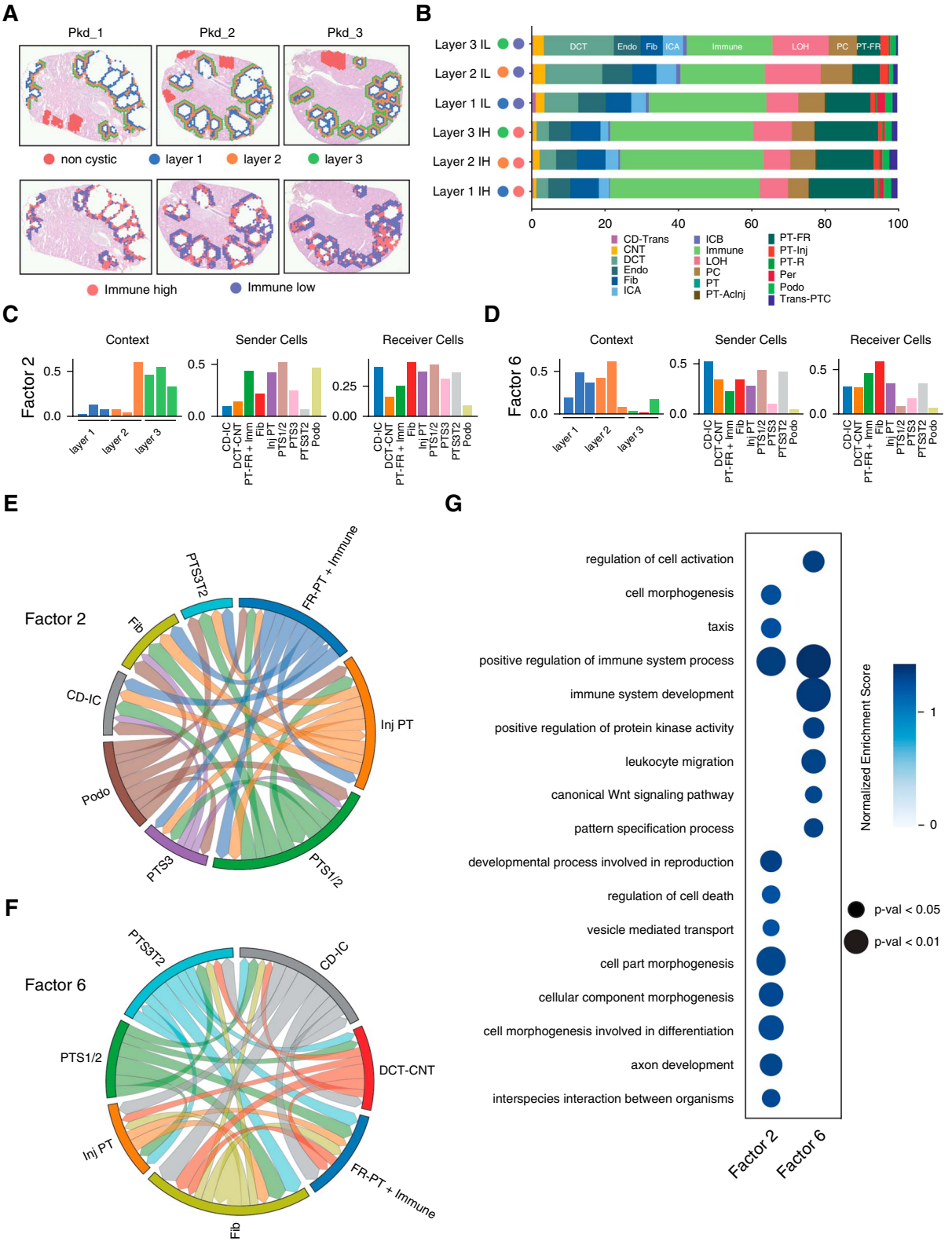


**Figure 5. Cell–cell communication events near cysts in immune-low spots.** (A) Left: Top: Visium spots colored according to their manual layer annotation (layer 1, layer 2, and layer 3) and spots in noncystic regions. All spots have a fixed center-to-center distance of 100 $\mu$m. Bottom: Visium spots colored according to their deconvolved immune content (immune-low and immune-high) and the lack of *Adgre1* expression. Noncystic spots were used to establish a gene expression threshold twice as high in the spots near cysts compared with those in noncystic regions. (B) Stacked bar plot displaying the fraction of annotated nuclei after deconvolution (as presented in Figure 2) in the different annotated areas. For easier visualization, PTS1, PTS2, PTS3, and PTS3T2 were grouped as PT. Immune

**Figure 5.** *Continued.* populations were grouped as Immune. Endothelial populations were grouped into Endo. TAL, ATL, DTL-ATL, and DTL were grouped as LOH. DCT and DCT-CNT were merged as DCT. (C and D) Context-dependent changes of cell communication patterns, and associated sender and receiver cells captured by Factor 2 (C) and Factor 6 (D) in immune-low spots (based on cell types presented in Figure 1). See Supplemental Figure 12 for a complete overview of the identified cell communication patterns. Context comprises immune-low spots in three layers around cysts shown in (A). (E and F) Chord plots displaying the cell–cell communication events between sender and receiver cell types for Factor 2 (C) and Factor 6 (D). Receiver cell types are displayed with an arrowhead at the end of the arch, which starts from sender cell types. (G) Dot plot visualization of the significant ($P$ value $< 0.05$) gene set enrichment results for the ligand and receptor pairs with the highest weights for Factor 2 and Factor 6. Shown are the significant redundancy-reduced GOBP terms, ranked on the $P$ value. FDR q-values are >0.05. See Supplemental Table 6 for a complete overview of the enriched GO terms and associated ligand-receptor pairs. FDR, false discovery rate.

patients,[76,77] showed weak expression in most control tubules with scattered strong clusters (Figure 6D). In ADPKD, Tenascin-C is mildly upregulated near cysts and strongly expressed in cyst-lining epithelium. Similarly, PTN[58,78] shows weak-to-moderate expression in distal tubules of control kidneys, while markedly upregulated in dilated tubules adjacent to cysts (Figure 6E).

In addition to spatial gene expression patterns (Supplemental Figure 20), evaluation of single-nucleus RNA-seq data from human ADPKD[15] tissue provides further validation of the expression patterns of these factors (Supplemental Figure 21). Consistently, elevated expression of COL4A1, MDK, ITGB1, CSF1, and TNC was observed in human ADPKD, particularly within renal epithelial and interstitial cell populations.

## Discussion

We present spatially resolved transcriptome data from healthy and polycystic mouse kidneys, mapping the distribution of various cell types. We analyzed spatial gene expression patterns and characterized the cyst microenvironment, revealing a specific cyst-associated gene signature and corresponding cell types. In addition, we investigated cell–cell communication near cysts and identified key ligand-receptor pairs related to immune system activation, differentiation, and morphogenesis. Prolonged stimulation of surrounding healthy epithelia by these factors could potentially promote disease progression.

Spatial gene expression analysis in cystic kidneys revealed an enrichment of genes involved in immune response, alongside reduced metabolic activity, consistent with our previous study from microdissected tissue microdomains adjacent to cysts.[10] The Visium platform provided an unbiased analysis of entire kidney sections, enhancing our understanding of both cystic and noncystic regions in PKD. We observed enrichment of PT-AcInj, PT-FR, PT-Inj, and PT-R cells in PKD, previously characterized in AKI.[34,79,80] Notably, trans-PT cells, proposed to precede PT-FR cell state in PKD,[16] were also enriched near cysts. Trans-PT cells were usually located near PT-FR cells, supporting this hypothesis.

In addition to failed repair and transitional proximal tubule cells, we observed accumulation of immune and stromal cell types within the PKD cyst microenvironment. Both immune cell modulation[35,81–86] and progressive kidney fibrosis[87–89] have been reported as central features of PKD pathogenesis. Although the roles of macrophages,[35,56,72,84,90] T lymphocytes,[83,86] and myofibroblasts[87,91] are well established, the contribution of failed repair[15,16] and transitional proximal tubule cells remains less well understood. In end-stage ADPKD, healthy proximal tubule cells appear to be replaced by PT-FR cells, which seem to originate primarily from injured tubules.[15] Here, we localize these cell types in tissue context and demonstrate their enrichment specifically within the cyst microenvironment, despite the scattered nature of *Pkd1* deletion. This finding suggests that the local microenvironmental cues may promote the accumulation, retention, or expansion of these cell populations, promoting disease progression. Close proximity of these cell types to cysts, along with the upregulation of genes related to inflammation and ECM remodeling, underscores the complex cellular interactions that shape the cystic niche in PKD.

Our cell communication analysis identified several ligands and receptors previously implicated in PKD/ADPKD progression, including SPP1,[16,73,92] macrophage migration inhibitory factor,[56] tumor necrosis factor ligand superfamily member 12 (Tnfsf12),[61] CSF1,[72] ITGB1,[68,88] and Collagen IV,[93] and several of the top-ranked ligand-receptor pairs were factors known to influence kidney cystic disease when modulated. For example, treatment with the macrophage migration inhibitory factor inhibitor ISO1 or knock-out of the *Mif* gene delayed cyst growth and ameliorated fibrosis in various mouse models, involving the receptor CD74, which also stood out in our cyst-associated gene signature analysis.[56,94] Cordido *et al.* demonstrated that administration of the cytokine TNF-related weak inducer of apoptosis (encoded by the *Tnfsf12* gene) accelerated cystogenesis in mice, whereas neutralizing anti-TNF–related weak inducer of apoptosis antibodies slowed disease progression.[61] Similarly, conditional inactivation of *Itgb1* in collecting ducts significantly inhibited cystogenesis and suppressed fibrosis. In addition, deletion of complement *C3*,[48] *Itga1*,[95] or knockdown of the *Notch3*[96] gene has been shown to reduce cystogenesis.

Beyond these well-established modulators of cystic disease, our analysis also revealed a broader set of signaling factors involved in immune modulation and inflammation (*Il34*,[49] *Cxcl12*,[50] *Ccl5*,[97] and *Vcam1*[67]), fibrosis and ECM remodeling (*Tnc*,[76,77] *Adam9/10*,[64,65] Collagens,[93,98] and *Thbs1/2*[99,100]), development, repair, and regeneration (*Angpt2*,[47] *Gas6*,[37] *Ptn*,[37,78] *Mdk*,[55,101,102] *Sfrp2*,[59] and *Wnt5a*[103,104]), and cell adhesion and signaling (*Sdc1*,[105] *Icam1*,[106] and Integrins[68,88]). Notably, several of these factors (*Ccl5, Sdc1,* and *Csf1r*) were also enriched in precystic kidneys and reported to be regulated by the polycystin complex in cilia,[70] suggesting a role in early

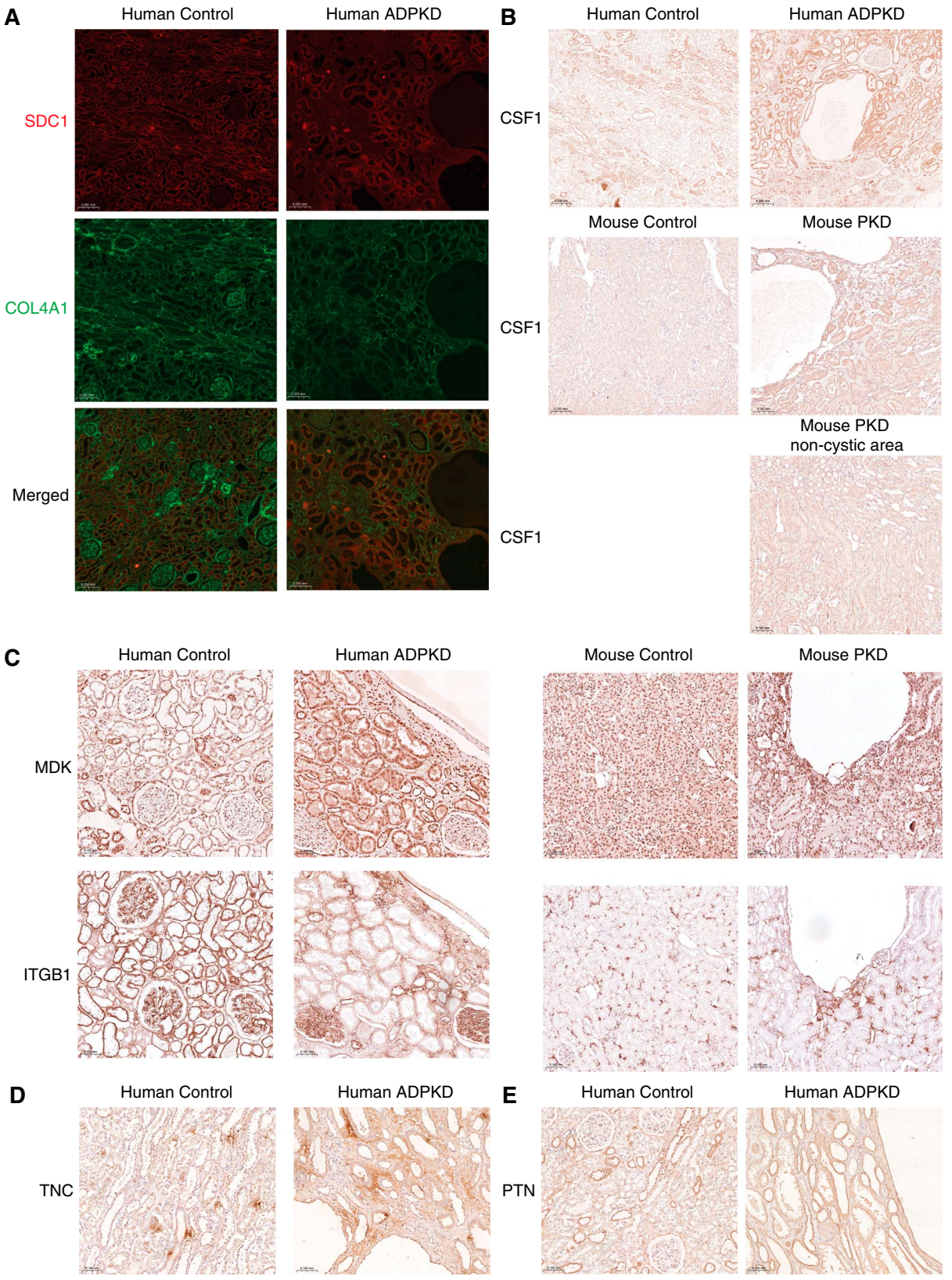


**Figure 6. IHC confirmed the expression of SDC1-COL4A1, CSF1, ITGB1-MDK, TNC, and PTN in cystic and healthy control kidneys.** (A) Representative immunofluorescence images showing colocalization of SDC1 and COL4A1 in human ADPKD and control kidneys. Scale bar: 0.200 mm (B) Representative immunohistochemistry images showing CSF1 expression in human ADPKD and mouse PKD compared with healthy controls. Scale bar: 0.200 mm for human tissues and 0.100 mm for mouse tissues. (C) Representative immunohistochemistry images showing ITGB1 and MDK expression in human ADPKD and mouse PKD compared with healthy controls.

**Figure 6.** *Continued.* Scale bar: 0.100 mm (D) Representative immunohistochemistry images showing TNC expression in human ADPKD and control kidneys. Scale bar: 0.100 mm (E) Representative immunohistochemistry images showing PTN expression in human ADPKD and control kidneys. Scale bar: 0.100 mm. ADPKD, autosomal dominant polycystic kidney disease; CSF1, colony-stimulating factor 1; MDK, Midkine; PTN, Pleiotrophin; TNC, Tenascin-C.

disease processes. Although our primary focus was on Factors 2 and 6 identified within immune-low spots, this study also provides a wealth of additional information, including interactions involving immune-high spots, offering valuable insights for future investigations.

To validate key interactions, we performed immunohistochemistry for a selected set of ligands and receptors (SDC1-COL4A1, CSF1, MDK-ITGB1, PTN, and TNC) primarily on end-stage human ADPKD tissue, due to antibody compatibility constraints. Although this may not fully reflect the spatial gene expression patterns observed in our mouse model with scattered *Pkd1* deletion, conserved expression of key factors supports the translational relevance of the mouse data. These findings highlight the presence of conserved signaling pathways across disease stages and species and point to potential therapeutic targets within the cystic microenvironment.

Sustained activation of developmental, proinflammatory, and profibrotic processes has been implicated in fibrosis development and kidney function loss.[107–109] The identification of (conserved) ligand-receptor interactions involved in these processes suggests that targeting such pathways may offer novel therapeutic strategies to mitigate fibrosis and preserve kidney function over time. Both spatial transcriptomic data and immunohistochemical validation indicate that, in some cases, elevated expression of either the ligand or its receptor appears to be the primary driver of signaling activity, while the corresponding interaction partner remains more broadly expressed. Adding to this complexity, many of these ligands and receptors engage with multiple interaction partners that are also enriched within the cystic microenvironment, potentially complicating therapeutic targeting. Further mechanistic studies will be essential to dissect these interactions and evaluate their therapeutic potential.

Although our study provides valuable insights into the spatial localization and ligand-receptor interactions within the PKD cyst microenvironment, some limitations should be acknowledged. First, the relatively low spatial resolution of the Visium platform may obscure finer cellular details and interactions. Future studies using higher-resolution spatial transcriptomics technologies, such as multiplexed error-robust fluorescence *in situ* hybridization or Slide-seq, could provide more precise mapping of cell types and signaling events. Second, the integration of paired single-cell RNA sequencing data would enhance cell-type resolution and allow for more accurate deconvolution of spatial transcriptomic signals. Third, although the number of biologic replicates is limited, our study focuses on the cystic microenvironment rather than direct comparisons between animals. Each of the three PKD kidneys contains >10 distinct cystic regions, enabling the identification of conserved cellular and molecular features across multiple cysts. Fourth, immunohistochemical validation on end-stage human tissue may not fully reflect early disease processes observed in the mouse model. Finally, although our ligand-receptor analysis identified numerous candidate interactions, functional validation remains necessary to confirm their roles in disease progression. Future work should focus on mechanistic studies of these pathways, ideally using time-resolved and cell-type–specific approaches, to further elucidate their therapeutic potential.

Despite these limitations, our data reveal that significant gene expression changes were predominantly observed within the cyst microenvironment, even in the context of scattered *Pkd1* inactivation. This niche is enriched with injury-associated and repair-associated cell states, myofibroblasts, and immune cells. The presence of cysts appears to establish an environment of chronic injury, characterized by inflammatory signaling and secretion of paracrine factors. The progressive nature of the disease impairs effective repair, leading to the accumulation of transforming and maladaptive cell types that may further exacerbate tissue damage and likely increase susceptibility to additional cyst formation.

Altogether, our study offers important contributions to the understanding of PKD by presenting a spatial transcriptomics dataset of whole kidney sections, enabling broad exploration of gene-specific spatial patterns in both WT and PKD kidneys. In addition, we spatially localized immune cells, injury repair–related cell types, and transitional proximal tubule cells, demonstrating their enrichment near cysts despite scattered *Pkd1* inactivation, further supporting the cystic snowball hypothesis. We also identified 45 cyst-associated signature genes, including well-known markers and novel candidates, with expression levels highest near cysts and decreasing with distance. Ligand-receptor interaction analysis revealed both established and novel factors in immune-low and immune-high regions, as well as their corresponding sending and receiving cells. Immunohistochemical validation confirmed markedly elevated expression of SDC1-COL4A1, CSF1, MDK-ITGB1, PTN, and TNC within the cyst microenvironment.

Collectively, our results reveal the cellular and molecular architecture of the cyst microenvironment and point to signaling interactions that may be therapeutically targeted to slow PKD progression.

## Disclosures

Disclosure forms, as provided by each author, are available with the online version of the article at http://links.lww.com/JSN/F467.

## Author Contributions

**Conceptualization:** Dorien J.M. Peters.
**Data curation:** Claudio Novella-Rausell.
**Formal analysis:** Claudio Novella-Rausell, Sevtap A. Yasinoglu.
**Funding acquisition:** Dorien J.M. Peters.
**Investigation:** Kyra L. Dijkstra, Claudio Novella-Rausell, Lisanne E. Wisse, Sevtap A. Yasinoglu.

**Software:** Claudio Novella-Rausell.
**Supervision:** Hans J. Baelde, Ahmed Mahfouz, Dorien J.M. Peters.
**Visualization:** Claudio Novella-Rausell, Sevtap A. Yasinoglu.
**Writing – original draft:** Sevtap A. Yasinoglu.
**Writing – review & editing:** Hans J. Baelde, Kyra L. Dijkstra, Ahmed Mahfouz, Claudio Novella-Rausell, Dorien J.M. Peters, Lisanne E. Wisse, Sevtap A. Yasinoglu.

### Funding

D.J.M. Peters: Nierstichting (19OP012) and HORIZON EUROPE Marie Sklodowska-Curie Actions (860977).

### Acknowledgments

The authors gratefully thank Laura Heezen and Pietro Spitali for their technical advice during the preparation of Visium tissue optimization and gene expression experiments. The authors also deeply appreciate Kelly Tsang's help with the stainings. In addition, the authors sincerely thank the Zimmerman lab for generously sharing their data and the associated metadata from their kidney immune atlas.

### Declarative Statements

All animal experiments were conducted in accordance with the NIH Guide for the Care and Use of Laboratory Animals or an equivalent standard that meets or exceeds the ethical and welfare requirements outlined in the NIH Guide. All protocols were approved by the appropriate institutional animal care and use committee.

### Data Availability Statements

Original data generated for the study are or will be made available in a public access repository upon publication. Data Type: Raw Data/Source Data; Software Source Code. Repository The sequencing files generated in this study are available at the sequence read archive accession number PRJNA1172747. The processed count matrices and corresponding H&E stainings are available at Zenodo (10.5281/zenodo.17279214). The original and injury-enriched versions of the single-cell MKA are available at https://github.com/nrclaudio/MKA. The analysis and figure-generation code used in this study is available at https://github.com/nrclaudio/spatial-pkd.

### Supplemental Material

This article contains the following supplemental material online at http://links.lww.com/JSN/F468, http://links.lww.com/JSN/F474, http://links.lww.com/JSN/F475, http://links.lww.com/JSN/F476, http://links.lww.com/JSN/F477, http://links.lww.com/JSN/F478, http://links.lww.com/JSN/F479, http://links.lww.com/JSN/F480, http://links.lww.com/JSN/F481.

Supplemental Table 1. DEGs cell-type clusters.

Supplemental Table 2. Meta-markers of the cell types present in the reference. Markers were used only for characterization and not for annotation or mapping.

Supplemental Table 3. Cell-type proportion Figures 1G and 2A, and the percentages of cell types from this study, PKD snRNA-seq dataset (Muto *et al.*, 2024), and the uni-IRI and unilateral ureteral obstruction scRNA-seq dataset (Li *et al.*, 2022).

Supplemental Table 4. Unsupervised spatial gene expression patterns.

Supplemental Table 5. Cell communication contexts, ligand-receptor pairs, sender-receiver cells IL.

Supplemental Table 6. GO terms Factor 2 and Factor 6.

Supplemental Table 7. Cell communication contexts, ligand-receptor pairs, sender-receiver cells immune high and immune low.

Supplemental Table 8. Differential gene expression analysis comparing immune-high and immune-low spots within the cyst microenvironment.

Supplemental Figure 1. Subclustering cluster 10, and distinction between PT-FR and PT-Inj clusters.

Supplemental Figure 2. Nuclei plot of deconvoluted spots for WT kidney.

Supplemental Figure 3. Nuclei plot of deconvoluted spots for Pkd_1 kidney.

Supplemental Figure 4. Nuclei plot of deconvoluted spots for Pkd_2 kidney.

Supplemental Figure 5. Nuclei plot of deconvoluted spots for Pkd_3 kidney.

Supplemental Figure 6. Nuclei plot of nuclei fib, Inj-PT, immune cells WT kidney.

Supplemental Figure 7. Nuclei plot of nuclei fib, Inj-PT, immune cells Pkd_1 kidney.

Supplemental Figure 8. Nuclei plot of nuclei fib, Inj-PT, immune cells Pkd_2 kidney.

Supplemental Figure 9. Nuclei plot of nuclei fib, Inj-PT, immune cells Pkd_3kidney.

Supplemental Figure 10. Correlation macrophages and immunohistochemical validation cell types.

Supplemental Figure 11. Unsupervised spatial gene expression patterns in WT kidney.

Supplemental Figure 12. Unsupervised spatial gene expression patterns in Pkd_1 kidney.

Supplemental Figure 13. Unsupervised spatial gene expression patterns in Pkd_2 kidney.

Supplemental Figure 14. Unsupervised spatial gene expression patterns in Pkd_3 kidney.

Supplemental Figure 15. Cell-type abundances to distance from cysts per kidney.

Supplemental Figure 16. Contextualized cell–cell communication patterns IL.

Supplemental Figure 17. Contextualized cell–cell communication patterns IH and IL.

Supplemental Figure 18. Cilia-dependent cyst activation pattern overlap with Top 20 ligand-receptor pairs IL spots.

Supplemental Figure 19. Close-up views of SDC1 ciliary localization and MDK nuclear staining.

Supplemental Figure 20. Spatial gene expression patterns of SDC1, COL4A1, ITGB1, MDK, SPP1, CSF1, CSF1R, IL34, TNC, PTN, and PTPRB projected on WT and PKD kidneys.

Supplemental Figure 21. Gene expression of validated key factors in human ADPKD and control cells from public snRNA-seq dataset.

Supplemental Figure 22. Spatial gene expression of cyst-associated signature genes projected on Pkd_2 kidney.

Supplemental Figure 23. Expression of cyst-associated signature genes among the different layers of spots surrounding cysts (layers 1, 2, and 3, as shown in Figure 5) and noncystic spots.

### References

1. Willey CJ, Blais JD, Hall AK, Krasa HB, Makin AJ, Czerwiec FS. Prevalence of autosomal dominant polycystic kidney disease in the European Union. *Nephrol Dial Transplant.* 2017;32(8):1356–1363. doi:10.1093/ndt/gfw240
2. Aung TT, Bhandari SK, Chen Q, et al. Autosomal dominant polycystic kidney disease prevalence among a racially diverse United States population, 2002 through 2018. *Kidney360.* 2021;2(12):2010–2015. doi:10.34067/kid.0004522021
3. Harris PC, Torres VE. Polycystic kidney disease. *Annual Rev Med.* 2009;60(1):321–337. doi:10.1146/annurev.med.60.101707.125712
4. Mochizuki T, Wu GQ, Hayashi T, et al. PKD2, a gene for polycystic kidney disease that encodes an integral membrane protein. *Science.* 1996;272(5266):1339–1342. doi:10.1126/science.272.5266.1339

5. Ward CJ, Peral B, Hughes J, et al. The polycystic kidney-disease-1 gene encodes a 14-Kb transcript and lies within a duplicated region on chromosome-16. *Cell.* 1994;77(6):881–894. doi:10.1038/ng0695-151
6. The polycystic kidney disease 1 gene encodes a 14 kb transcript and lies within a duplicated region on chromosome 16. *Cell.* 1994;77(6):881–894. doi:10.1016/0092-8674(94)90137-6
7. Lavu S, Vaughan LE, Senum SR, et al. The value of genotypic and imaging information to predict functional and structural outcomes in ADPKD. *JCI Insight.* 2020;5(15):e138724. doi:10.1172/jci.insight.138724
8. Torres VE, Chapman AB, Devuyst O, et al. Multicenter study of long-term safety of tolvaptan in later-stage autosomal dominant polycystic kidney disease. *Clin J Am Soc Nephrol.* 2020;16(1):48–58. doi:10.2215/Cjn.10250620
9. Leonhard WN, Zandbergen M, Veraar K, et al. Scattered deletion of PKD1 in kidneys causes a cystic snowball effect and recapitulates polycystic kidney disease. *J Am Soc Nephrol.* 2015;26(6):1322–1333. doi:10.1681/ASN.2013080864
10. Yasinoglu SA, Kuipers TB, Suidgeest E, et al. Transcriptomic profiling of polycystic kidney disease identifies paracrine factors in the early cyst microenvironment. *Biochim Biophys Acta Mol Basis Dis.* 2024;1870(2):166987. doi:10.1016/j.bbadis.2023.166987
11. Li LX, Zhang X, Zhang H, et al. Single-cell and cellchat resolution identifies collecting duct cell subsets and their communications with adjacent cells in PKD kidneys. *Cells.* 2022;12(1):45. doi:10.3390/cells12010045
12. Malas TB, Formica C, Leonhard WN, et al. Meta-analysis of polycystic kidney disease expression profiles defines strong involvement of injury repair processes (vol 312, pg F806, 2017). *Am J Physiol Renal Physiol.* 2018;314(1):F140. doi:10.1152/ajprenal.zh2-8408-corr.2017
13. Kunnen SJ, Malas TB, Formica C, Leonhard WN, t Hoen PAC, Peters DJM. Comparative transcriptomics of shear stress treated Pkd1(-/-) cells and pre-cystic kidneys reveals pathways involved in early polycystic kidney disease. *Biomed Pharmacother.* 2018;108:1123–1134. doi:10.1016/j.biopha.2018.07.178
14. Malas TB, Leonhard WN, Bange H, et al. Prioritization of novel ADPKD drug candidates from disease-stage specific gene expression profiles. *EBioMedicine.* 2020;51:102585. doi:10.1016/j.ebiom.2019.11.046
15. Muto Y, Dixon EE, Yoshimura Y, et al. Defining cellular complexity in human autosomal dominant polycystic kidney disease by multimodal single cell analysis. *Nat Commun.* 2022;13(1):6497. doi:10.1038/s41467-022-34255-z
16. Muto Y, Yoshimura Y, Wu H, et al. Multiomics profiling of mouse polycystic kidney disease progression at a single-cell resolution. *Proc Natl Acad Sci U S A.* 2024;121(43):e2410830121. doi:10.1073/pnas.2410830121
17. Lantinga-van Leeuwen IS, Leonhard WN, van der Wal A, Breuning MH, de Heer E, Peters DJ. Kidney-specific inactivation of the Pkd1 gene induces rapid cyst formation in developing kidneys and a slow onset of disease in adult mice. *Hum Mol Genet.* 2007;16(24):3188–3196. doi:10.1093/hmg/ddm299
18. Wolf FA, Angerer P, Theis FJ. SCANPY: large-scale single-cell gene expression data analysis. *Genome Biol.* 2018;19(1):15. doi:10.1186/s13059-017-1382-0
19. Traag VA, Waltman L, Van Eck NJ. From Louvain to Leiden: guaranteeing well-connected communities. *Scientific Rep.* 2019;9(1):5233. doi:10.1038/s41598-019-41695-z
20. Korotkevich G, Sukhov V, Budin N, Shpak B, Artyomov MN, Sergushichev A. Fast gene set enrichment analysis. *biorxiv.* Preprint posted online February 1, 2021. doi:10.1101/060012
21. Castanza AS, Recla JM, Eby D, Thorvaldsdóttir H, Bult CJ, Mesirov JP. Extending support for mouse data in the molecular signatures database (MSigDB). *Nat Methods.* 2023;20(11):1619–1620. doi:10.1038/s41592-023-02014-7
22. Sayols S. Rrvgo: a Bioconductor package for interpreting lists of gene ontology terms. *MicroPubl Biol.* 2023. doi:10.17912/micropub.biology.000811
23. Argelaguet R, Arnol D, Bredikhin D, et al. MOFA+: a statistical framework for comprehensive integration of multi-modal single-cell data. *Genome Biol.* 2020;21(1):111. doi:10.1186/s13059-020-02015-1
24. Velten B, Braunger JM, Argelaguet R, et al. Identifying temporal and spatial patterns of variation from multimodal data using MEFISTO. *Nat Methods.* 2022;19(2):179–186. doi:10.1038/s41592-021-01343-9
25. Biancalani T, Scalia G, Buffoni L, et al. Deep learning and alignment of spatially resolved single-cell transcriptomes with tangram. *Nat Methods.* 2021;18(11):1352–1362. doi:10.1038/s41592-021-01264-7
26. Novella-Rausell C, Grudniewska M, Peters DJM, Mahfouz A. A comprehensive mouse kidney atlas enables rare cell population characterization and robust marker discovery. *iScience.* 2023;26(6):106877. doi:10.1016/j.isci.2023.106877
27. Zimmerman KA, Bentley MR, Lever JM, et al. Single-cell RNA sequencing identifies candidate renal resident macrophage gene expression signatures across species. *J Am Soc Nephrol.* 2019;30(5):767–781. doi:10.1681/ASN.2018090931
28. Li H, Dixon EE, Wu H, Humphreys BD. Comprehensive single-cell transcriptional profiling defines shared and unique epithelial injury responses during kidney fibrosis. *Cell Metab.* 2022;34(12):1977–1998.e9. doi:10.1016/j.cmet.2022.09.026
29. Lopez R, Regier J, Cole MB, Jordan MI, Yosef N. Deep generative modeling for single-cell transcriptomics. *Nat Methods.* 2018;15(12):1053–1058. doi:10.1038/s41592-018-0229-2
30. Xu C, Lopez R, Mehlman E, Regier J, Jordan MI, Yosef N. Probabilistic harmonization and annotation of single-cell transcriptomics data with deep generative models. *Mol Syst Biol.* 2021;17(1):e9620. doi:10.15252/msb.20209620
31. Stuart T, Butler A, Hoffman P, et al. Comprehensive integration of single-cell data. *Cell.* 2019;177(7):1888–1902.e21. doi:10.1016/j.cell.2019.05.031
32. Dimitrov D, Schäfer PSL, Farr E, et al. LIANA1: An All-In-One Cell-Cell Communication Framework. *biorxiv.* Preprint posted online August 21, 2023. doi:10.1101/2023.08.19.553863
33. Balzer MS, Rohacs T, Susztak K. How many cell types are in the kidney and what do they do? *Annu Rev Physiol.* 2022;84:507–531. doi:10.1146/annurev-physiol-052521-121841
34. Kirita Y, Wu H, Uchimura K, Wilson PC, Humphreys BD. Cell profiling of mouse acute kidney injury reveals conserved cellular responses to injury. *Proc Natl Acad Sci U S A.* 2020;117(27):15874–15883. doi:10.1073/pnas.2005477117
35. Song CJ, Li Z, Ahmed UKB, et al. A comprehensive immune cell atlas of cystic kidney disease reveals the involvement of adaptive immune cells in injury-mediated cyst progression in mice. *J Am Soc Nephrol.* 2022;33(4):747–768. doi:10.1681/ASN.2021030278
36. Muto Y, Yoshimura Y, Wu H, et al. Multi-omics profiling of mouse polycystic kidney disease progression at a single cell resolution. *Proc Natl Acad Sci U S A.* 2024;121(43):e2410830121. doi:10.1073/pnas.2410830121
37. Wang Z, Deng Q, Gu Y, et al. Integrated single-nucleus sequencing and spatial architecture analysis identified distinct injured-proximal tubular types in calculi rats. *Cell Biosci.* 2023;13(1):92. doi:10.1186/s13578-023-01041-3
38. Tang Y, Zhang Y, Li X, et al. Immune landscape and the key role of APOE+ monocytes of lupus nephritis under the single-cell and spatial transcriptional vista. *Clin Transl Med.* 2023;13(4):e1237. doi:10.1002/ctm2.1237
39. Hoeft K, Schaefer GJL, Kim H, et al. Platelet-instructed SPP1(+) macrophages drive myofibroblast activation in fibrosis in a CXCL4-dependent manner. *Cell Rep.* 2023;42(2):112131. doi:10.1016/j.celrep.2023.112131
40. Dvergsten J, Manivel JC, Correa-Rotter R, Rosenberg ME. Expression of clusterin in human renal diseases. *Kidney Int.* 1994;45(3):828–835. doi:10.1038/ki.1994.109
41. Valkova N, Yunis R, Mak SK, Kang K, Kültz D. Nek8 mutation causes overexpression of galectin-1, sorcin, and vimentin and accumulation of the major urinary protein in renal cysts of jck mice. *Mol Cell Proteomics.* 2005;4(7):1009–1018. doi:10.1074/mcp.M500091-MCP200
42. Lai X, Bacallao RL, Blazer-Yost BL, Hong D, Mason SB, Witzmann FA. Characterization of the renal cyst fluid

proteome in autosomal dominant polycystic kidney disease (ADPKD) patients. *Proteomics Clin Appl.* 2008;2(7-8):1140–1152. doi:10.1002/prca.200780140
43. Wang W, Mei C, Tang B, et al. Aberrant expression of SPARC and its impact on proliferation and apoptosis in ADPKD cyst-lining epithelia. *Nephrol Dial Transplant.* 2006;21(5):1278–1288. doi:10.1093/ndt/gfk036
44. Lei J, Sun P, Sheng J, Wang H, Xie Y, Song J. The intricate role of annexin A2 in kidney: a comprehensive review. *Ren Fail.* 2023;45(2):2273427. doi:10.1080/0886022x.2023.2273427
45. Izquierdo MC, Martin-Cleary C, Fernandez-Fernandez B, et al. CXCL16 in kidney and cardiovascular injury. *Cytokine Growth Factor Rev.* 2014;25(3):317–325. doi:10.1016/j.cytogfr.2014.04.002
46. Jiang N, Huang R, Zhang J, et al. TIMP2 mediates endoplasmic reticulum stress contributing to sepsis-induced acute kidney injury. *FASEB J.* 2022;36(4):e22228. doi:10.1096/fj.202101555RR
47. Coffelt SB, Chen Y-Y, Muthana M, et al. Angiopoietin 2 stimulates TIE2-expressing monocytes to suppress T cell activation and to promote regulatory T cell expansion. *J Immunol.* 2011;186(7):4183–4190. doi:10.4049/jimmunol.1002802
48. Bin S, Yoo M, Molinari P, et al. Reduced decay-accelerating factor expression promotes complement-mediated cystogenesis in murine ADPKD. *JCI Insight.* 2024;9(12):e175220. doi:10.1172/jci.insight.175220
49. Lin W, Xu D, Austin CD, et al. Function of CSF1 and IL34 in macrophage homeostasis, inflammation, and cancer. *Front Immunol.* 2019;10:2019. doi:10.3389/fimmu.2019.02019
50. Song A, Jiang A, Xiong W, Zhang C. The role of CXCL12 in kidney diseases: a friend or foe? *Kidney Dis (Basel).* 2021;7(3):176–185. doi:10.1159/000514913
51. Richmond J, Tuzova M, Cruikshank W, Center D. Regulation of cellular processes by interleukin-16 in homeostasis and cancer. *J Cell Physiol.* 2014;229(2):139–147. doi:10.1002/jcp.24441
52. Yıldırım B, Kulak K, Bilir A. Midkine: a cancer biomarker candidate and innovative therapeutic approaches. *Eur J Breast Health.* 2024;20(3):167–177. doi:10.4274/ejbh.galenos.2024.2024-4-7
53. Xu C, Chen J, Liang L, et al. Midkine promotes renal fibrosis by stabilizing C/EBPβ to facilitate endothelial-mesenchymal transition. *Commun Biol.* 2024;7(1):544. doi:10.1038/s42003-024-06154-0
54. Weckbach LT, Gola A, Winkelmann M, et al. The cytokine midkine supports neutrophil trafficking during acute inflammation by promoting adhesion via β2 integrins (CD11/CD18). *Blood.* 2014;123(12):1887–1896. doi:10.1182/blood-2013-06-510875
55. Sato W, Yuzawa Y, Kadomatsu K, et al. Midkine expression in the course of nephrogenesis and its role in ischaemic reperfusion injury. *Nephrol Dial Transplant.* 2002;17(suppl 9):52–54. doi:10.1093/ndt/17.suppl_9.52
56. Chen L, Zhou X, Fan LX, et al. Macrophage migration inhibitory factor promotes cyst growth in polycystic kidney disease. *The J Clin Invest.* 2015;125(6):2399–2412. doi:10.1172/Jci80467
57. Wang X. Pleiotrophin: activity and mechanism. *Adv Clin Chem.* 2020;98(98):51–89. doi:10.1016/bs.acc.2020.02.003
58. Sakurai H, Bush KT, Nigam SK. Identification of pleiotrophin as a mesenchymal factor involved in ureteric bud branching morphogenesis. *Development.* 2001;128(17):3283–3293. doi:10.1242/dev.128.17.3283
59. Lv D, Lin Z, Liao X, et al. Sfrp2 promotes renal dysfunction of diabetic kidney disease via modulating Fzd5-induced cytosolic calcium ion concentration and CaMKII/Mek/Erk pathway in mesangial cells. *Biochim Biophys Acta Mol Basis Dis.* 2024;1870(2):166933. doi:10.1016/j.bbadis.2023.166933
60. Diab L, Al Kattar S, Oueini N, et al. Syndecan-1: a key player in health and disease. *Immunogenetics.* 2024;77(1):9. doi:10.1007/s00251-024-01366-4
61. Cordido A, Nunez-Gonzalez L, Martinez-Moreno JM, et al. TWEAK signaling pathway blockade slows cyst growth and disease progression in autosomal dominant polycystic kidney disease. *J Am Soc Nephrol.* 2021;32(8):1913–1932. doi:10.1681/ASN.2020071094
62. Zhou D, Fu H, Zhang L, et al. Tubule-derived wnts are required for fibroblast activation and kidney fibrosis. *J Am Soc Nephrol.* 2017;28(8):2322–2336. doi:10.1681/ASN.2016080902
63. Spanjer AI, Baarsma HA, Oostenbrink LM, et al. TGF-β-induced profibrotic signaling is regulated in part by the WNT receptor Frizzled-8. *FASEB J.* 2016;30(5):1823–1835. doi:10.1096/fj.201500129
64. Mahimkar RM, Visaya O, Pollock AS, Lovett DH. The disintegrin domain of ADAM9: a ligand for multiple beta1 renal integrins. *Biochem J.* 2005;385(Pt 2):461–468. doi:10.1042/bj20041133
65. Li B, Zhu C, Dong L, et al. ADAM10 mediates ectopic proximal tubule development and renal fibrosis through notch signalling. *J Pathol.* 2020;252(3):274–289. doi:10.1002/path.5517
66. Luo H, Broux B, Wang X, et al. EphrinB1 and EphrinB2 regulate T cell chemotaxis and migration in experimental autoimmune encephalomyelitis and multiple sclerosis. *Neurobiol Dis.* 2016;91:292–306. doi:10.1016/j.nbd.2016.03.013.
67. Melchinger I, Guo K, Li X, Guo J, Cantley LG, Xu L. VCAM-1 mediates proximal tubule-immune cell cross talk in failed tubule recovery during AKI-to-CKD transition. *Am J Physiol Renal Physiol.* 2024;327(4):F610–F622. doi:10.1152/ajprenal.00076.2024
68. Zhang Y, Reif G, Wallace DP. Extracellular matrix, integrins, and focal adhesion signaling in polycystic kidney disease. *Cell Signal.* 2020;72:109646. doi:10.1016/j.cellsig.2020.109646
69. Peng H, Yang M, Feng K, Lv Q, Zhang Y. Semaphorin 3C (Sema3C) reshapes stromal microenvironment to promote hepatocellular carcinoma progression. *Signal Transduct Target Ther.* 2024;9(1):169. doi:10.1038/s41392-024-01887-0
70. Zhang C, Rehman M, Tian X, et al. Glis2 is an early effector of polycystin signaling and a target for therapy in polycystic kidney disease. *Nat Commun.* 2024;15(1):3698. doi:10.1038/s41467-024-48025-6
71. Guo S, Wu X, Lei T, et al. The role and therapeutic value of Syndecan-1 in cancer metastasis and drug resistance. *Front Cell Dev Biol.* 2021;9:784983. doi:10.3389/fcell.2021.784983
72. Zimmerman KA, Song CJ, Li Z, et al. Tissue-resident macrophages promote renal cystic disease. *J Am Soc Nephrol.* 2019;30(10):1841–1856. doi:10.1681/ASN.2018080810
73. Jansson KP, Kuluva J, Zhang S, et al. Osteopontin deletion attenuates cyst growth but exacerbates fibrosis in mice with cystic kidney disease. *Physiol Rep.* 2024;12(17):e70038. doi:10.14814/phy2.70038
74. Şalaru DL, Arsenescu-Georgescu C, Chatzikyrkou C, Karagiannis J, Fischer A, Mertens PR. Midkine, a heparin-binding growth factor, and its roles in atherogenesis and inflammatory kidney diseases. *Nephrol Dial Transplant.* 2016;31(11):1781–1787. doi:10.1093/ndt/gfw083
75. Shibata Y, Muramatsu T, Hirai M, et al. Nuclear targeting by the growth factor midkine. *Mol Cell Biol.* 2002;22(19):6788–6796. doi:10.1128/MCB.22.19.6788-6796.2002
76. Fu HY, Tian Y, Zhou LL, et al. Tenascin-C is a major component of the fibrogenic niche in kidney fibrosis. *J Am Soc Nephrol.* 2017;28(3):785–801. doi:10.1681/ASN.2016020165
77. Zhu H, Liao J, Zhou X, et al. Tenascin-C promotes acute kidney injury to chronic kidney disease progression by impairing tubular integrity via αvβ6 integrin signaling. *Kidney Int.* 2020;97(5):1017–1031. doi:10.1016/j.kint.2020.01.026
78. Yeh HJ, He YY, Xu J, Hsu CY, Deuel TF. Upregulation of pleiotrophin gene expression in developing microvasculature, macrophages, and astrocytes after acute ischemic brain injury. *J Neurosci.* 1998;18(10):3699–3707. doi:10.1523/JNEUROSCI.18-10-03699.1998
79. Gerhardt LMS, Liu J, Koppitch K, Cippà PE, McMahon AP. Single-nuclear transcriptomics reveals diversity of proximal tubule cell states in a dynamic response to acute kidney injury. *Proc Natl Acad Sci U S A.* 2021;118(27):e2026684118. doi:10.1073/pnas.2026684118

80. Muto Y, Dixon EE, Yoshimura Y, et al. Epigenetic reprogramming driving successful and failed repair in acute kidney injury. *Sci Adv.* 2024;10(32):eado2849. doi:10.1126/sciadv.ado2849
81. Petitprez F, Levy S, Sun C-M, et al. The murine microenvironment cell population counter method to estimate abundance of tissue-infiltrating immune and stromal cell populations in murine samples using gene expression. *Genome Med.* 2020;12(1):86. doi:10.1186/s13073-020-00783-w
82. Mrug M, Zhou J, Woo Y, et al. Overexpression of innate immune response genes in a model of recessive polycystic kidney disease. *Kidney Int.* 2008;73(1):63–76. doi:10.1038/sj.ki.5002627
83. Kleczko EK, Marsh KH, Tyler LC, et al. CD8(+) T cells modulate autosomal dominant polycystic kidney disease progression. *Kidney Int.* 2018;94(6):1127–1140. doi:10.1016/j.kint.2018.06.025
84. Swenson-Fields KI, Vivian CJ, Salah SM, et al. Macrophages promote polycystic kidney disease progression. *Kidney Int.* 2013;83(5):855–864. doi:10.1038/ki.2012.446
85. Zimmerman KA, Hopp K, Mrug M. Role of chemokines, innate and adaptive immunity. *Cell Signal.* 2020;73:109647. doi:10.1016/j.cellsig.2020.109647
86. Kleczko EK, Nguyen DT, Marsh KH, et al. Immune checkpoint activity regulates polycystic kidney disease progression. *JCI Insight.* 2023;8(12):e161318. doi:10.1172/jci.insight.161318
87. Dwivedi N, Jamadar A, Mathew S, Fields TA, Rao R. Myofibroblast depletion reduces kidney cyst growth and fibrosis in autosomal dominant polycystic kidney disease. *Kidney Int.* 2023;103(1):144–155. doi:10.1016/j.kint.2022.08.036
88. Lee K, Boctor S, Barisoni LM, Gusella GL. Inactivation of integrin-$\beta$1 prevents the development of polycystic kidney disease after the loss of polycystin-1. *J Am Soc Nephrol.* 2015;26(4):888–895. doi:10.1681/ASN.2013111179
89. Okada H, Ban S, Nagao S, Takahashi H, Suzuki H, Neilson EG. Progressive renal fibrosis in murine polycystic kidney disease: an immunohistochemical observation. *Kidney Int.* 2000;58(2):587–597. doi:10.1046/j.1523-1755.2000.00205.x
90. Karihaloo A, Koraishy F, Huen SC, et al. Macrophages promote cyst growth in polycystic kidney disease. *J Am Soc Nephrol.* 2011;22(10):1809–1814. doi:10.1681/ASN.2011010084
91. Gomez IG, Roach AM, Nakagawa N, et al. TWEAK-Fn14 signaling activates myofibroblasts to drive progression of fibrotic kidney disease. *J Am Soc Nephrol.* 2016;27(12):3639–3652. doi:10.1681/ASN.2015111227
92. Cowley BD Jr., Ricardo SD, Nagao S, Diamond JR. Increased renal expression of monocyte chemoattractant protein-1 and osteopontin in ADPKD in rats. *Kidney Int.* 2001;60(6):2087–2096. doi:10.1046/j.1523-1755.2001.00065.x
93. Schäfer K, Bader M, Gretz N, Oberbäumer I, Bachmann S. Focal overexpression of collagen IV characterizes the initiation of epithelial changes in polycystic kidney disease. *Exp Nephrol.* 1994;2(3):190–195. PMID: 7922272
94. Zhou JX, Cheng AS, Chen L, et al. CD74 promotes cyst growth and renal fibrosis in autosomal dominant polycystic kidney disease. *Cells.* 2024;13(6):489. doi:10.3390/cells13060489
95. Grenier C, Lin IH, Peters D, Pozzi A, Lennon R, Naylor RW. Integrin alpha1 beta1 promotes interstitial fibrosis in a mouse model of polycystic kidney disease. *bioRxiv.* Preprint posted online October 21, 2024. doi:10.1101/2024.10.18.619080
96. Su L, Chen T, Hu H, et al. Notch3 as a novel therapeutic target for the treatment of ADPKD by regulating cell proliferation and renal cyst development. *Biochem Pharmacol.* 2024;224:116200. doi:10.1016/j.bcp.2024.116200
97. Cockwell P, Calderwood JW, Brooks CJ, Chakravorty SJ, Savage CO. Chemoattraction of T cells expressing CCR5, CXCR3 and CX3CR1 by proximal tubular epithelial cell chemokines. *Nephrol Dial Transplant.* 2002;17(5):734–744. doi:10.1093/ndt/17.5.734
98. Gulati A, Sevillano AM, Praga M, et al. Collagen IV gene mutations in adults with bilateral renal cysts and CKD. *Kidney Int Rep.* 2020;5(1):103–108. doi:10.1016/j.ekir.2019.09.004
99. Daniel C, Wiede J, Krutzsch HC, et al. Thrombospondin-1 is a major activator of TGF-beta in fibrotic renal disease in the rat in vivo. *Kidney Int.* 2004;65(2):459–468. doi:10.1111/j.1523-1755.2004.00395.x
100. Hugo C, Daniel C. Thrombospondin in renal disease. *Nephron Exp Nephrol.* 2009;111(3):e61–e66. doi:10.1159/000198235
101. Qiu L, Hyink DP, Gans WH, Amsler K, Wilson PD, Burrow CR. Midkine promotes selective expansion of the nephrogenic mesenchyme during kidney organogenesis. *Organogenesis.* 2004;1(1):14–21. doi:10.4161/org.1.1.979
102. Vilar J, Lalou C, Van Huyen J-PD, et al. Midkine is involved in kidney development and in its regulation by retinoids. *J Am Soc Nephrol.* 2002;13(3):668–676. doi:10.1681/ASN.V133668
103. Yun K, Ajima R, Sharma N, et al. Non-canonical Wnt5a/Ror2 signaling regulates kidney morphogenesis by controlling intermediate mesoderm extension. *Hum Mol Genet.* 2014;23(25):6807–6814. doi:10.1093/hmg/ddu397
104. Nishita M, Qiao S, Miyamoto M, et al. Role of Wnt5a-Ror2 signaling in morphogenesis of the metanephric mesenchyme during ureteric budding. *Mol Cell Biol.* 2014;34(16):3096–3105. doi:10.1128/mcb.00491-14
105. Herum KM, Lunde IG, Skrbic B, et al. Syndecan-4 is a key determinant of collagen cross-linking and passive myocardial stiffness in the pressure-overloaded heart. *Cardiovasc Res.* 2015;106(2):217–226. doi:10.1093/cvr/cvv002
106. Chow J, Hartley RB, Jagger C, Dilly SA. ICAM-1 expression in renal disease. *J Clin Pathol.* 1992;45(10):880–884. doi:10.1136/jcp.45.10.880
107. Edeling M, Ragi G, Huang S, Pavenstädt H, Susztak K. Developmental signalling pathways in renal fibrosis: the roles of Notch, Wnt and Hedgehog. *Nat Rev Nephrol.* 2016;12(7):426–439. doi:10.1038/nrneph.2016.54
108. Zhou D, Tan RJ, Fu HY, Liu YH. Wnt/$\beta$-catenin signaling in kidney injury and repair: a double-edged sword. *Lab Invest.* 2016;96(2):156–167. doi:10.1038/labinvest.2015.153
109. Xie Y, Su N, Yang J, et al. FGF/FGFR signaling in health and disease. *Signal Transduct Target Ther.* 2020;5(1):181. doi:10.1038/s41392-020-00222-7


## AFFILIATIONS


[1]Department of Human Genetics, Leiden University Medical Center, Leiden, The Netherlands
[2]Department of Pathology, Leiden University Medical Center, Leiden, The Netherlands
[3]Delft Bioinformatics Lab, TU Delft, Delft, The Netherlands